J. Fluid Mech. (2016), *vol.* 800, *pp.* 278–306.

doi:10.1017/jfm.2016.392

Exact solutions to non-classical steady nozzle flows of Bethe–Zel'dovich–Thompson fluids

Alberto Guardone[1,†] **and Davide Vimercati**[1]

[1]Department of Aerospace Science and Technology, Politecnico di Milano, Via La Masa 34, 20156 Milano, Italy

(Received 13 November 2015; revised 2 May 2016; accepted 6 June 2016; first published online 1 July 2016)

Steady nozzle flows of Bethe–Zel'dovich–Thompson fluids – substances exhibiting non-classical gasdynamic behaviour in a finite vapour-phase thermodynamic region in close proximity to the liquid–vapour saturation curve – are examined. Non-classical flow features include rarefaction shock waves, shock waves with either upstream or downstream sonic states and split shocks. Exact solutions for a mono-component single-phase fluid expanding from a reservoir into a stationary atmosphere through a conventional converging–diverging nozzle are determined within the quasi-one-dimensional inviscid flow approximation. The novel analytical approach makes it possible to elucidate the connection between the adiabatic, possibly non-isentropic flow field and the underlying local isentropic-flow features, including the possible qualitative alterations in passing through shock waves. Contrary to previous predictions based on isentropic-flow inspection, shock disintegration is found to occur also from reservoir states corresponding to a single sonic point. The global layout of the flow configurations produced by a monotonic decrease in the ambient pressure, namely the functioning regime, is examined for reservoir conditions resulting in single-phase flows. Accordingly, a classification of steady nozzle flows into 10 different functioning regimes is proposed. Flow conditions determining the transition between the different classes of flow are investigated and each functioning regime is associated with the corresponding thermodynamic region of reservoir states.

Key words: compressible flows, gas dynamics, shock waves

1. Introduction

The steady flow of gases through a variable area duct is a prototypical problem in fluid dynamics. The theory of nozzle flows of ideal gases is well-established and exploited in many applications that involve gases operating in dilute conditions. However, compressible-fluid flows in the vapour-phase thermodynamic region near liquid–vapour equilibrium can exhibit a significant departure from ideal-gas behaviour.

† Email address for correspondence: alberto.guardone@polimi.it

Bethe (1942), Zel'dovich (1946), Weyl (1949) and Thompson (1971) first pointed out the paramount role of the so-called fundamental derivative of gasdynamics, namely

$$\Gamma = \frac{v^3}{2c^2}\left(\frac{\partial^2 P}{\partial v^2}\right)_s, \tag{1.1}$$

in delineating the dynamic behaviour of compressible-fluid flows in non-ideal conditions, see also Hayes (1958). In the above expression P is the pressure, v the specific volume, s the specific entropy per unit mass and c, $c^2 = -v^2(\partial P/\partial v)_s$, is the speed of sound. Classical gasdynamics is rooted in the assumption that the fundamental derivative is positive and it is exemplified by the process of shock formation via the coalescence of planar finite-amplitude compression waves. Conversely, non-classical gasdynamic phenomena are expected to occur in flows evolving in the regime of negative ($\Gamma < 0$) or mixed nonlinearity ($\Gamma \lessgtr 0$). Noteworthy examples of non-classical phenomena include the formation of expansion shock waves (see Thompson 1971; Thompson & Lambrakis 1973; Cramer & Kluwick 1984; Cramer & Sen 1986), of shock waves with either upstream or downstream sonic states (see Thompson & Lambrakis 1973; Cramer & Sen 1987) and of composite and split waves (see Menikoff & Plohr 1989; Bates & Montgomery 1999). Note that such unconventional wave patterns cannot exist in dilute gases with constant specific heats, nor in any substances for which the fundamental derivative is always positive.

The possibility that $\Gamma < 0$ within a certain thermodynamic region was first explored independently by Bethe (1942) and Zel'dovich (1946) for van der Waals gases. As discussed in these investigations and later by Thompson (1971), Lambrakis & Thompson (1972) and Thompson & Lambrakis (1973), non-classical gasdynamic behaviour is expected to occur in fluid flows of substances with sufficiently large specific heats (e.g. high molecular complexity) and in close proximity to the liquid–vapour saturation curve. Thanks to the significant contributions by these authors, fluids exhibiting negative nonlinearity in the single-phase vapour region are now commonly referred to as Bethe–Zel'dovich–Thompson (BZT) fluids. Substantial theoretical and numerical effort has been accomplished in the investigation of the non-classical gasdynamic region for candidate BZT fluids, such as hydrocarbons, perfluorocarbons and siloxanes; see Thompson & Lambrakis (1973), Cramer (1991), Colonna & Silva (2003), Guardone & Argrow (2005), Colonna, Guardone & Nannan (2007) and references therein.

Nozzle flows of fluids experiencing mixed nonlinearity have been widely examined in the scientific literature. Thompson (1971) first investigated the role of Γ in accelerating flows through a sonic throat, demonstrating that an anti-throat is required to accelerate to supersonic speed if $\Gamma < 0$. Cramer & Best (1991) examined steady isentropic flows of fluids in the dense-gas regime, focusing on the relation between the Mach number and the density. The main result is that the Mach number no longer increases monotonically with decreasing density if $\Gamma < 1$. In addition, if $\Gamma < 0$, the number of sonic points may increase from one only to three. Steady quasi-one-dimensional flows containing multiple sonic points were investigated also by Chandrasekar & Prasad (1991) and Kluwick (1993) in the context of transonic flows. Their work pointed out the existence of unconventional shocks, namely expansion and sonic shocks, in the neighbourhood of the throat of a converging–diverging nozzle. Moreover, these authors provided examples of reservoir states not allowing for shock-free flows expanding to arbitrarily large Mach numbers. The reference work of Cramer & Fry (1993) shed further light on the admissible flows of BZT fluids in

a conventional converging–diverging nozzle. Solutions accounting for the entropy rise across shock waves were produced for the first time, by employing a shock fitting technique based on a sixth-order Runge–Kutta scheme. Two types of non-classical nozzle flows were introduced, in addition to the classical case (e.g. nozzle flows qualitatively similar to those of ideal gases). In a complete expansion from rest to arbitrarily large exit Mach numbers, Type-1 flows include a rarefaction shock in the diverging section of the nozzle. Conversely, in Type-2 nozzle flows a rarefaction shock is observed in the converging section of the nozzle.

The present study is aimed at complementing the theoretical framework delineated by the above-mentioned investigators, in order to provide further insights into the theory of steady nozzle flows of BZT fluids. The main focus is on the possible flow configurations that occur in a conventional converging–diverging nozzle connected to a reservoir with fixed thermodynamic state. The layout of the exact solutions produced by monotonically decreasing values of the ambient pressure determines the so-called functioning regime. As many as 10 functioning regimes are singled out, which also include the two classes of flow introduced by Cramer & Fry (1993), whose findings are confirmed by the present analysis. The leading goal of this work is to investigate the connection between reservoir conditions and functioning regimes. To this end, the precise conditions leading to the transition between different functioning regimes are determined.

The accurate characterization of nozzle flows in the negative-Γ region is of theoretical as well as practical interest, inasmuch as it is expected to support and facilitate the design of machinery possibly operating in non-classical conditions, such as organic Rankine cycle (ORC) power systems (see Brown & Argrow 2000; Colonna *et al.* 2015) or high-temperature heat pumps (see Zamfirescu & Dincer 2009). Valuable information may also be inferred to support the experimental attempt to demonstrate the existence of non-classical gasdynamic phenomena. In this respect, despite the undeniable theoretical progress in the field of compressible-fluid dynamics, no experimental evidence of non-classical behaviour is available to date. Among the notable attempts to observe these phenomena, the experiment by Borisov *et al.* (1983) was adversely interpreted at a later stage (see Cramer & Sen 1986; Kutateladze, Nakoryakov & Borisov 1987; Thompson 1991; Fergason *et al.* 2001) and the ones performed by Fergason, Guardone & Argrow (2003) and Guardone (2007) failed due to the thermal decomposition of the working fluid. Recently, the Flexible Asymmetric Shock Tube (FAST) was designed and commissioned at Delft University of Technology, the Netherlands, with the aim of generating non-classical rarefaction shock waves in dense vapours of organic fluids (see Colonna *et al.* 2008). Preliminary experiments (see Mathijssen *et al.* 2015) were successfully performed on rarefaction waves in the non-ideal classical regime of siloxane fluid D_6 (dodecamethylcyclohexasiloxane, $C_{12}H_{36}O_6Si_6$). The Test-Rig for Organic VApours (TROVA) at Politecnico di Milano (see Spinelli *et al.* 2010, 2013; Guardone, Spinelli & Dossena 2013) was specifically designed and commissioned to investigate non-ideal compressible nozzle flows of pure organic fluids for ORC applications. Ongoing research activities in the TROVA include the investigation of non-classical nozzle flows of mixtures of siloxane fluids.

The present work is organized as follows. In § 2, the governing equations of quasi-one-dimensional flows are recalled and the general properties of isentropic flows are delineated. Exact solutions corresponding to 10 different functioning regimes in a converging–diverging nozzle are outlined in § 3 using the simple yet qualitatively correct van der Waals model. In § 4, the correspondence of each of the functioning regimes to reservoir thermodynamic states is identified. Section 5 presents the concluding remarks.

2. Non-classical nozzle flows: general analysis

In this section, the basic properties of steady nozzle flows are briefly recalled. Specific flow conditions are selected to show the anomalous behaviour caused by thermodynamic states featuring negative nonlinearity. The general framework for inspection of isentropic nozzle flows is established by analysing the Mach number variation with density and the phase plane. The convenient concept of the isentropic pattern is also introduced.

2.1. *Problem formulation*

In the present study, the quasi-one-dimensional approximation is used to model the steady flow of a mono-component single-phase fluid through a converging–diverging nozzle. The quasi-one-dimensional governing equations for smooth, i.e. shock-free, flows are the well-known algebraic equations enforcing the conservation of mass, of total enthalpy and entropy, namely

$$\rho u A(x) = \text{const.}, \tag{2.1a}$$

$$h + \tfrac{1}{2}u^2 = \text{const.}, \tag{2.1b}$$

$$s = \text{const.}, \tag{2.1c}$$

where ρ, u, h are the fluid density, velocity and specific enthalpy per unit mass, respectively, and $A(x)$ is the known cross-sectional area distribution along the axial coordinate x.

Discontinuous solutions including shock waves are accounted for by means of the well-known Rankine–Hugoniot jump relations. The locus of thermodynamic states that can possibly be connected by a shock wave, if drawn in the P–v plane, is referred to as the shock adiabat. If the pre-shock state is fixed, the shock adiabat determines the relation between the pressure and the specific volume of the post-shock state. However, the post-shock state satisfying the jump conditions for a given pre-shock state is, in general, not unique. The Rankine–Hugoniot relations must be supplemented with suitable admissibility criteria in order to rule out unphysical solutions. One sufficient condition is that shock waves arise as limits of travelling-wave profiles including viscosity and heat conduction (see Menikoff & Plohr 1989; Kluwick 2001). This admissibility criterion has a direct and convenient graphical interpretation: the straight segment connecting the pre-shock and post-shock states in the P–v plane (commonly referred to as the Rayleigh line) must be located either completely above or completely below the shock adiabat centred on the pre-shock state. In the first case, the shock wave carries a positive pressure jump (compression shock); in the second one the shock carries a negative pressure jump (expansion or rarefaction shock). Note that shock waves admitting viscous profiles also satisfy the well-known entropy condition $s_B \geqslant s_A$ and the speed ordering relation $M_A \geqslant 1 \geqslant M_B$, where subscripts A and B denote pre-shock and post-shock quantities, respectively (Lax 1957; Oleinik 1959).

In order to complete the problem, a suitable thermodynamic model of the fluid must be specified. In this work, we consider fluids described by the model of van der Waals (1873) with constant isochoric heat capacity c_v, namely

$$P(T, v) = \frac{RT}{v - b} - \frac{a}{v^2}, \quad c_v = \text{const.}, \tag{2.2a,b}$$

where R is the gas constant, T is the temperature and the constants a and b account for the excluded volume and for the intermolecular forces, respectively. Thanks to its simplicity, the van der Waals model with constant c_v (also referred to as the polytropic van der Waals model) has frequently been employed in studies on negative and mixed nonlinearities (see, e.g. Cramer & Sen 1986; Cramer 1991; Argrow 1996; Brown & Argrow 1997; Müller & Voß 2006). Indeed, as pointed out by many authors (see, e.g. Thompson & Lambrakis 1973; Kluwick 2001; Guardone, Vigevano & Argrow 2004; Guardone & Argrow 2005), the polytropic van der Waals model predicts the correct qualitative behaviour in the thermodynamic region of interest in this work, though it is admittedly less accurate with respect to more complex thermodynamic models (see Martin & Hou 1955; Martin, Kapoor & De Nevers 1959; Peng & Robinson 1976; Span & Wagner 2003*a*,*b*).

Moreover, analytical equations of state, including the van der Waals model considered here, fail to predict the fluid thermodynamics in the very close proximity of the liquid–vapour critical point. The divergence of properties near the critical point is properly described in terms of scaling laws, see for example the scaling laws proposed by Levelt-Sengers (1970), Levelt-Sengers, Greer & Sengers (1976) and Levelt-Sengers, Morrison & Chang (1983). Non-classical gasdynamic in the critical region was studied by Emanuel (1996) and more recently by Nannan, Guardone & Colonna (2013, 2014) and Nannan *et al.* (2016). In particular, in Nannan *et al.* (2013), a comparison is made between analytical thermodynamic models and scaling laws in terms of the predicted values of Γ and a significant departure was observed only in very close proximity to the critical point ($|T/T_c - 1| < 0.01$). The thermodynamic region of interest here is sufficiently far from the critical point to rely on analytical models and the analysis of nozzle flows in very close proximity to the liquid–vapour critical point is left for future investigations.

2.2. *Isentropic flow*

According to the governing equations (2.1), the mass flow rate $\dot{m} = \rho u A(x)$ and the total enthalpy $h^t = h + u^2/2$ are uniform both in shock-free and in shocked flows. The entropy s, on the other hand, is piece-wise uniform with finite jumps occurring across shock waves. Therefore, most non-classical effects occurring in quasi-1D steady nozzle flows can be explained in a comprehensive manner by examining the basic properties of isentropic flows with constant total enthalpy.

We start by commenting on the relation between the Mach number $M = u/c = \sqrt{2(h^t - h)}/c$ and the density in non-ideal compressible-fluid flows. Following Cramer & Best (1991), the first derivative of M is recast in non-dimensional form as

$$J = \frac{\rho}{M}\frac{\mathrm{d}M}{\mathrm{d}\rho} = 1 - \Gamma - \frac{1}{M^2}. \tag{2.3}$$

In flows of fluids with $\Gamma > 1$ (perfect gases, for instance), the Mach number always decreases upon isentropic compression. Conversely, in fluid flows exhibiting $\Gamma < 1$, the Mach number can possibly increase with density. The variation of the Mach number along exemplary isentropic flows computed from the van der Waals model with $c_v/R = 50$ is sketched in figure 1(*a*). The current fluid model specifications correspond to a BZT fluid and will be used throughout the present work. The M–ρ diagram shown in figure 1(*a*) is generated for a fixed value of the total enthalpy. Thus, each curve corresponds to a different entropy value along the same isenthalpic line $h = h^t$. Isentropes in figure 1(*a*) intersect the liquid–vapour phase boundary along

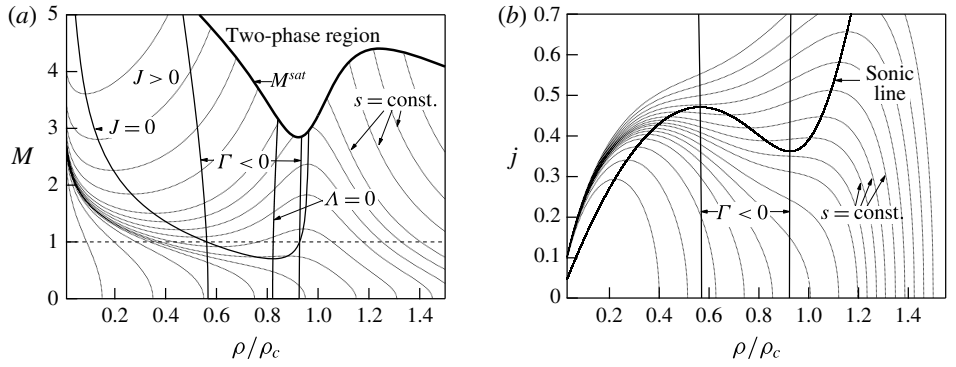

FIGURE 1. Variation of the Mach number (*a*) and of the mass flux function (*b*) along exemplary isentropes, as computed from the polytropic van der Waals model with $c_v/R = 50$. The total enthalpy is constant, $h^t = h(1.0182P_c, v_c)$.

curve labelled M^{sat}. A wide portion of the saturated vapour boundary of the fluid considered is retrograde (see Thompson, Carofano & Kim 1986; Menikoff & Plohr 1989), meaning that isentropes cross the phase boundary from the mixed towards the pure phase, in the direction of decreasing density. However, all isentropes eventually enter the two-phase region crossing a non-retrograde saturated phase boundary. The intersection with the non-retrograde portion of the saturated vapour boundary occurs at such low density values, compared to those characterizing the thermodynamic region of interest in this work, that it is reasonable to assume that isentropes cross saturation boundaries only if $s < s_{vle}$, where s_{vle} denotes the isentrope tangent to the vapour dome. The present analysis is limited to the single-phase portions of any given isentrope. Two-phase effects, as well as critical point phenomena which affect near-to-critical isentropes, are outside the scope of this work.

The locus $J = 0$ in figure 1(*a*) gathers all stationary points in the Mach number-density plot and its general form can be explained by analysing the evolution of Γ along isentropes featuring $\Gamma < 1$ (see, e.g. Bethe 1942; Zel'dovich 1946; Thompson & Lambrakis 1973). On these isentropes, $\Gamma - 1$ has only two zeros with a local minimum in between, where $\Lambda = (\partial\Gamma/\partial\rho)_s$ vanishes. We differentiate (2.3) to obtain, after evaluation at $J = 0$,

$$\left.\frac{\mathrm{d}^2 M}{\mathrm{d}\rho^2}\right|_{J=0} = -\frac{M}{\rho}\Lambda. \tag{2.4}$$

Thus, with reference to figure 1(*a*), stationary points of the Mach number located at higher densities ($\Lambda > 0$) and at lower densities ($\Lambda < 0$) of the $\Lambda = 0$ locus are local maxima and minima, respectively.

Isentropes corresponding to sufficiently large stagnation densities must cross the $J > 0$ region. We restrict the discussion to those curves that remain in the single-phase region during a full expansion from stagnation conditions to vacuum. In this case, isentropes entering the $J > 0$ region exhibit both a local minimum and a local maximum of the Mach number. If the latter occurs at sufficiently high Mach numbers, the flow remains supersonic upon further expansion. On the other hand, if the local maximum is only slightly supersonic, the flow becomes subsonic inside the $J > 0$ region. As a result, the selected isentrope exhibits three sonic points. By decreasing

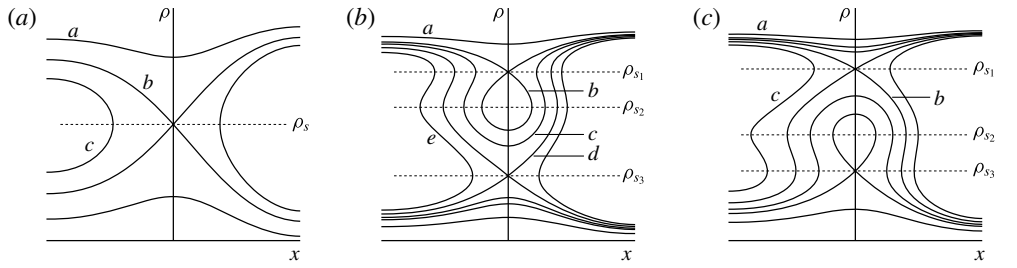

FIGURE 2. Phase planes for selected isentropes featuring (*a*) one sonic point and (*b*,*c*) three sonic points upon isentropic expansion with constant total enthalpy. Dashed segments denote sonic values of the density, ordered as $\rho_{s_3} < \rho_{s_2} < \rho_{s_1}$. If one sonic point only is present, it is specified as ρ_s. (*b*) The lowest of the sonic densities corresponds to the global maximum of the related mass flux function. (*c*) The largest of the sonic densities corresponds to the global maximum of the related mass flux function.

the stagnation density, the two stationary points become subsonic and eventually merge in a stationary inflection point. If the stagnation density is further decreased, the Mach number ultimately becomes a monotone decreasing function of the density.

Next, we consider the variation of the mass flux function $j = \rho\sqrt{2(h^t - h)}$ in isentropic flows with constant total enthalpy. Firstly, j varies with ρ according to

$$\frac{1}{c}\frac{\mathrm{d}j}{\mathrm{d}\rho} = \frac{M^2 - 1}{M}. \tag{2.5}$$

Thus, the mass flux function increases (decreases) upon supersonic (subsonic) isentropic compression and sonic points are extrema. In addition, given that

$$\left.\frac{\rho}{c}\frac{\mathrm{d}^2 j}{\mathrm{d}\rho^2}\right|_{M=1} = -2\Gamma, \tag{2.6}$$

a sonic point is a local maximum, minimum or stationary inflection point of the mass flux if Γ is positive, negative or null at that point, respectively. A similar analysis was performed by Kluwick (1993, 2004), albeit in the context of small perturbations in transonic flows. Figure 1(*b*) illustrates exemplary mass flux functions corresponding to different entropy values chosen along the isenthalpic locus $h = h^t$.

In this respect, it is instructive to analyse the phase plane related to such isentropic flows, i.e. the contour plot of the mass flow rate $\dot{m} = jA(x)$ in the ρ–x plane. In this study, all plots refer to a converging–diverging nozzle described by a fifth-order polynomial, whose coefficients are computed to set the inlet area $A_i = 1.2$, the throat area $A_t = 1$ and an exit area $A_e = 1.5$, and by imposing that the inlet, the throat and the exit stations are stationary points of the area distribution.

Isentropes containing a single sonic point generate saddle-shaped phase planes, see figure 2(*a*). The relevant value

$$\dot{m}_c = \max_{\rho} j(\rho;\, s,\, h^t) \min_{x} A(x) \tag{2.7}$$

corresponds to the saddle point and is referred to as the critical mass flow rate. In the present case $\dot{m}_c = j(\rho_s;\, s,\, h^t)A_t$, where ρ_s is the (unique) sonic density. Given that we

are interested in the expansion from a reservoir, we will naturally focus on subsonic inlet conditions. Curves such as a in figure 2(a) display $\dot{m} < \dot{m}_c$ and result in strictly subsonic flows. The curve labelled b in figure 2(a) corresponds to $\dot{m} = \dot{m}_c$. Subsonic–supersonic transition is possible, as well as completely subsonic flow with sonic throat. Along curves such as curve c, which display $\dot{m} > \dot{m}_c$, sonic conditions occur upstream of the throat and the flow cannot be continued beyond this point. These trajectories have no physical relevance in steady isentropic flows discharging from a still reservoir.

The flows we are mainly interested in are those associated with isentropes including three sonic points. Phase planes related to such isentropes exhibit two saddle points with a local minimum in between. Given the following ordering for the sonic values of the density,

$$\rho_{s_3} < \rho_{s_2} < \rho_{s_1}, \tag{2.8}$$

two different categories of phase plane were defined by Cramer & Fry (1993), depending on which of the local maxima is the global one.

The case $\dot{m}_c = j(\rho_{s_3};\, s,\, h^t)A_t$ is depicted in figure 2(b). We follow Cramer & Fry (1993) in referring to this kind of non-classical phase plane as Type-2. In figure 2(b), in addition to the possible cases presented in figure 2(a), there exist feasible paths (e.g. contour lines going from the inlet section to the outlet section) in which sonic conditions are encountered either upstream or downstream of the throat. For example, if $\dot{m} = j(\rho_{s_1};\, s,\, h^t)A_t$, the curve labelled b is generated which corresponds to a flow that is sonic both at the throat ($\rho = \rho_{s_1}$) and in the diverging section ($\rho = \rho_{s_2}$). However, in the latter sonic condition, the slope $\mathrm{d}\rho/\mathrm{d}x$ goes to infinity and the trajectory has a turning point. Therefore, the flow cannot be continued isentropically beyond this sonic point. Curves labelled c ($\dot{m} < \dot{m}_c$) and d ($\dot{m} = \dot{m}_c$) also include multiple sonic points and, such as in case b, these paths cannot be accomplished in an isentropic flow.

Figure 2(c) describes the case $\dot{m}_c = j(\rho_{s_1};\, s,\, h^t)A_t$, which is referred to as a Type-1 phase plane in accordance with the nomenclature proposed by Cramer & Fry (1993). Significant trajectories with subsonic inlet are those of type a ($\dot{m} < \dot{m}_c$) and b ($\dot{m} = \dot{m}_c$). The latter cannot be continued beyond sonic point ρ_{s_2}, which occurs downstream of the throat. By using an approximate isentropic model, i.e. neglecting the entropy rise across shock waves, Cramer & Fry (1993) depicted expected flow configurations including several non-classical shock waves. The phase plane analysis predicts the formation of non-classical flow fields along paths including three sonic points, see also Kluwick (1993). Trajectories such as b, c and d in figure 2(b) or b in figure 2(c) are indeed realizable and represent branches of shocked flows, yet the insertion of sonic shocks is required where sonic conditions occur upstream or downstream of the throat. In such cases, flows with arbitrarily large exit Mach numbers cannot be realized isentropically, as is the case in classical nozzle flows of ideal gases.

2.3. *Isentropic patterns*

The general properties of a quasi-1D isentropic flow, such as the number of sonic points and the layout of the corresponding phase plane, delineate a so-called isentropic pattern. We propose a classification of quasi-1D isentropic flows into five different isentropic patterns, as detailed in table 1. In the following, symbol $\mathscr{S}$ will be used to denote isentropic patterns. We regard any isentropic flow as ideal, and we denote the corresponding ideal isentropic pattern as $\mathscr{S}^I$, if the Mach number monotonically increases with decreasing density in a complete expansion from stagnation. Therefore,

Isentropic pattern	Number of sonic points	$J\|_{M<1}$	$J\|_{M>1}$	$\max_\rho j$
$\mathscr{S}^{I}$	1	$J<0$	$J<0$	ρ_s
$\mathscr{S}^{NI}$	1	$J<0$	$J\lesseqgtr 0$	ρ_s
$\mathscr{S}^{NC}_3$	1	$J\lesseqgtr 0$	$J<0$	ρ_s
$\mathscr{S}^{NC}_2$	3	$J\lesseqgtr 0$	$J\lesseqgtr 0$	ρ_{s_3}
$\mathscr{S}^{NC}_1$	3	$J\lesseqgtr 0$	$J\lesseqgtr 0$	ρ_{s_1}

TABLE 1. Description of isentropic patterns. In the presence of multiple sonic points, the corresponding densities are ordered as $\rho_{s_3}<\rho_{s_2}<\rho_{s_1}$. If one sonic point only is present, it is specified as ρ_s.

such flows exhibit a single sonic point. The monotonicity of the Mach number may break down in the supersonic regime of flows evolving under non-ideal conditions, namely $0<\Gamma<1$. The corresponding non-ideal pattern is denoted as $\mathscr{S}^{NI}$. Three non-classical isentropic patterns are distinguished. Firstly, if Γ becomes negative, the Mach number may increase with density also in the subsonic regime. Pattern $\mathscr{S}^{NC}_3$ refers to isentropes with a single sonic point and $J>0$ for some density values in a subsonic flow. Following Cramer & Fry (1993), isentropic flows including three sonic point are classified according to the layout of the related phase plane. We formally define patterns of $\mathscr{S}^{NC}_2$ type as those exhibiting a phase plane qualitatively similar to that of figure 2(*b*); isentropic pattern $\mathscr{S}^{NC}_1$ is associated to the phase plane of figure 2(*c*).

Isentropic patterns are separated by so-called transitional isentropic patterns. Isentropes corresponding to transitional isentropic patterns are sketched in figure 3(*a*,*b*) for a constant value of the total enthalpy (the same used in the computation of figure 1). The limiting curve for $\mathscr{S}^{NI}/\mathscr{S}^{NC}_1$ transition includes a simple ($J\neq 0$) high-density sonic point and a non-simple ($J=0$) low-density sonic point. The latter splits into two distinct simple sonic points (isentropic pattern $\mathscr{S}^{NC}_1$) if the stagnation density is slightly decreased. Next, when $\rho_{s_3}c(\rho_{s_3},\,s)=\rho_{s_1}c(\rho_{s_1},\,s)$ the mass flux function has two distinct global maxima and transition $\mathscr{S}^{NC}_1/\mathscr{S}^{NC}_2$ occurs. With decreasing stagnation density, the two high-density sonic points approach each other and eventually merge in the transitional isentropic flow $\mathscr{S}^{NC}_2/\mathscr{S}^{NC}_3$. Finally, the limiting curve for $\mathscr{S}^{NC}_3/\mathscr{S}^{I}$ transition intersects the locus $J=0$ at its minimum ($J=0$ and $\Lambda=0$ simultaneously).

The value of the total enthalpy that was used for the computation of figures 1 and 3 is such that all different isentropic patterns possibly arise. By varying the total enthalpy and gathering the values of stagnation states corresponding to transitional isentropic patterns, one ultimately obtains a thermodynamic map as shown, e.g. for the P–v diagram in figure 4. The map in figure 4 allows one to determine the isentropic pattern resulting from a given set of stagnation thermodynamic conditions. Due to the assumption of single-phase flows, the thermodynamic region of interest is bounded by the saturated vapour boundary if $s<s_{vle}$. In this case, we can consider the vapour-phase portion of the isentrope and, in spite of the possibility that the region $\Gamma<0$ is crossed, pattern $\mathscr{S}^{I}$ necessarily occurs. Note that this is a major difference compared to non-classical unsteady flows. In a steady flow, non-classical effects are due to the possibly non-monotone evolution of the Mach number, which arises in the nearly sonic or supersonic regime. Therefore, the corresponding stagnation states must be located at density values higher than those associated with the negative-Γ region. If $s_{vle}<s<s_\tau$, where s_τ denotes the isentrope tangent to the locus $\Gamma=0$,

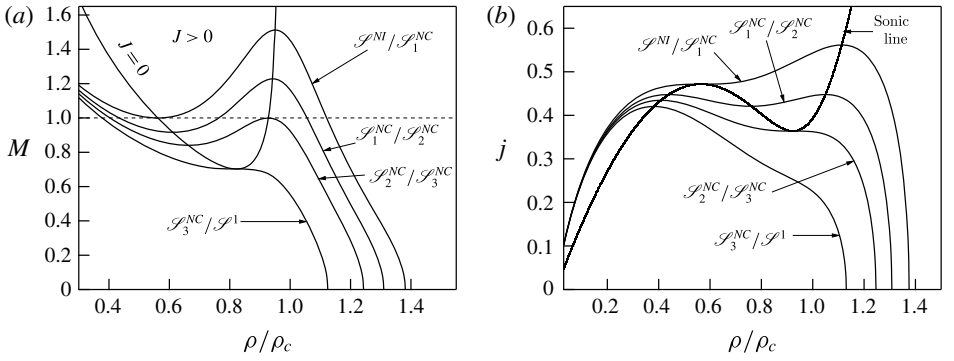

FIGURE 3. Variation of (*a*) Mach number and (*b*) mass flux function with density for transitional isentropic flows, computed from the polytropic van der Waals model with $c_v/R = 50$. The total enthalpy is constant and equal to the value employed in the computation of figure 1.

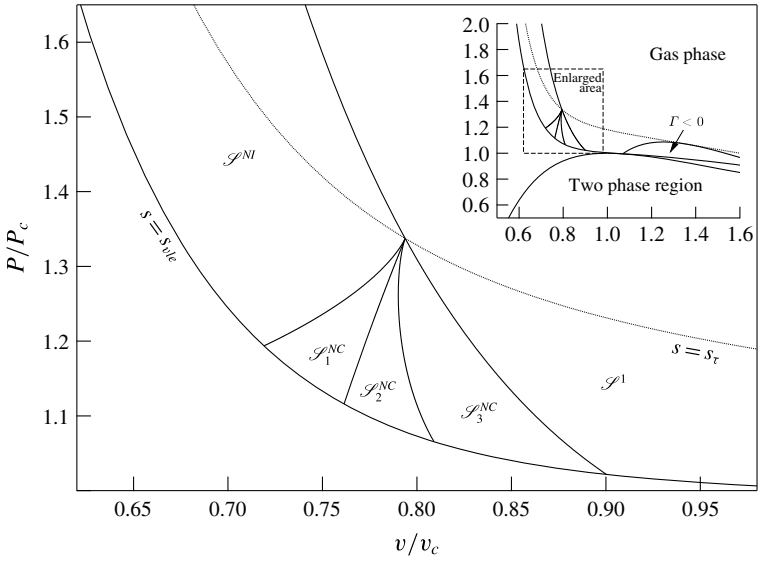

FIGURE 4. Thermodynamic map of stagnation states related to each isentropic pattern, computed from the van der Waals polytropic model with $c_v/R = 50$. Curves labelled $s = s_{vle}$ and $s = s_\tau$ represent the isentropes tangent to the vapour dome and to the $\Gamma = 0$ locus, respectively.

each class of isentropic flow can be observed depending on the stagnation state. In the direction of increasing density, patterns $\mathscr{S}^1$, $\mathscr{S}_3^{NC}$, $\mathscr{S}_2^{NC}$, $\mathscr{S}_1^{NC}$ and $\mathscr{S}^{NI}$ are encountered. With increasing values of s, the region of stagnation states leading to non-classical isentropic patterns shrinks and the corresponding transitional curves ultimately coincide in a single thermodynamic state when $s = s_\tau$. Along isentropes featuring $0 < \Gamma < 1$, the Mach number may exhibit a non-monotone profile in the supersonic regime, because $J > 0$ if $\Gamma < 1$ and M is sufficiently large. Accordingly, either $\mathscr{S}^{NI}$ or $\mathscr{S}^{I}$ is possible depending on the stagnation state. The transitional locus

$\mathscr{S}^{NI}/\mathscr{S}^{I}$ is constructed in the same way as $\mathscr{S}_3^{NC}/\mathscr{S}^{I}$, i.e. it comprises all stagnation states corresponding to isentropes that intersect the locus $J=0$ at its minimum (with the difference that for $\mathscr{S}^{NI}/\mathscr{S}^{I}$ said minimum is supersonic). If $\Gamma > 1$ everywhere along the reference isentrope, the Mach number is a monotone decreasing function of the density and pattern $\mathscr{S}^{I}$ only can take place.

The identification of the different types of isentropic flow behaviour is essential prior to the construction of general solutions to nozzle flows, which possibly include shock waves. Indeed, smooth branches of any quasi-1D flow can be associated locally with an isentropic pattern. The entropy jump across shock waves results in a shift of the pertinent isentropic curve and can possibly result in the qualitative modification of the flow behaviour, i.e. in a transition of the isentropic pattern. The second law of thermodynamics dictates the direction in which this process can possibly occur. The stagnation density decreases with increasing entropy at constant enthalpy,

$$\left(\frac{\partial \rho}{\partial s}\right)_h = -\frac{\rho T(1+G)}{c^2} < 0, \tag{2.9}$$

where $G = v(\partial P/\partial e)_v$ is the Grüneisen parameter, which we assume to be positive here throughout. Menikoff & Plohr (1989) discussed the assumption of $G > 0$ for real materials, which is implied by a positive value of the coefficient of thermal expansion, a condition fulfilled by most fluids of interest (with the relevant exception of water at 0 °C and 1 bar, see Bethe 1942). Therefore, with reference to figure 3(*a*,*b*), transitions of the isentropic pattern occur in the direction of increasing entropy as follows:

$$\mathscr{S}^{NI} \to \mathscr{S}_1^{NC} \to \mathscr{S}_2^{NC} \to \mathscr{S}_3^{NC} \to \mathscr{S}^{I}. \tag{2.10}$$

Evidently, the transition is not required to occur between two consecutive isentropic patterns (e.g. $\mathscr{S}^{NI} \to \mathscr{S}_2^{NC}$ or $\mathscr{S}_3^{NC} \to \mathscr{S}^{I}$ are admissible transitions). One of the most relevant consequences of the entropy rise across a shock wave is the possible change in the number of sonic points, for the phase planes featuring one only and three sonic points are structurally different, see § 2.2. The number of sonic points may either decrease (following an e.g. $\mathscr{S}_1^{NC} \to \mathscr{S}_3^{NC}$ transition), or increase (e.g. $\mathscr{S}^{NI} \to \mathscr{S}_2^{NC}$). In addition, from previous investigations it was inferred that non-classical flow fields are associated with reservoir conditions of type $\mathscr{S}_1^{NC}$ and $\mathscr{S}_2^{NC}$. The present analysis suggests that non-classical flow configurations are expected also from reservoir conditions featuring a single sonic point, namely $\mathscr{S}^{NI}$, because of the possible transition $\mathscr{S}^{NI} \to \mathscr{S}_1^{NC}$, $\mathscr{S}_2^{NC}$. The latter claim is confirmed in the following section.

3. Functioning regimes in a converging–diverging nozzle

In this section we single out the possible quasi-1D flows of BZT fluids in a converging–diverging nozzle. The nozzle is regarded as a discharging device between a reservoir with known, fixed conditions and a stationary atmosphere with known ambient pressure P_a (the ambient pressure will be, in general, different from the pressure P_e observed at the exit section). Thus, we will naturally focus on subsonic inlet conditions.

The mass balance equation $j(\rho; s, h^t)A(x) - \dot{m} = 0$ provides an implicit definition of $\rho(x; s, h^t, \dot{m})$. The three parameters which need to be specified, namely the entropy, the total enthalpy and the mass flow rate, are related to the reservoir conditions (for instance, the total enthalpy is uniform throughout the nozzle and equal to the reservoir

Isentropic pattern of the reservoir conditions	Possible functioning regimes
$\mathscr{S}^{I}$	$\mathscr{R}^{I}$
$\mathscr{S}^{NC}_{3}$	$\mathscr{R}^{NC}_{3}$
$\mathscr{S}^{NC}_{2}$	$\mathscr{R}^{NC}_{2}$, $\mathscr{R}^{NC}_{1}$
$\mathscr{S}^{NC}_{1}$	$\mathscr{R}^{NC}_{1}$
$\mathscr{S}^{NI}$	$\mathscr{R}^{NI}$, $\mathscr{R}^{NC}_{0}$

TABLE 2. Summary of the functioning regimes in a converging–diverging nozzle produced by different isentropic patterns of the reservoir conditions.

enthalpy) and to the value of the ambient pressure. From these parameters, the density distribution inside the nozzle is determined by means of standard root-finding algorithms, up to arbitrary accuracy. Our approach is based on computing the inverse of the mass flux function with respect to its first argument, along with enforcing the Rankine–Hugoniot jump relations across shock waves, if any are present. Note that the mass balance equation will yield at least two different roots if $\dot{m} < \dot{m}_c$, whereby each root is included in a subsonic or supersonic branch of the related mass flux function (sonic points are extrema). Smooth transition from subsonic to supersonic flow can be attained only at the throat of the nozzle, because if $M = 1$ and $A'(x) \neq 0$, $\mathrm{d}\rho/\mathrm{d}x$ becomes infinite and, in general, a shock is required to continue the flow. Non-smooth supersonic to subsonic transition is, of course, possible across a shock wave.

3.1. *Functioning regimes: overview*

We will investigate quasi-1D steady nozzle flows by examining the dependence of the flow field on the ambient pressure P_a, or similarly on the ambient to reservoir pressure ratio $\beta = P_a/P_r$, for given reservoir conditions (subscript r will be used to denote reservoir quantities). When the range $0 < \beta \leqslant 1$ is spanned, a specific sequence of solutions is observed, which together delineate the so-called functioning regime, to be referred to as $\mathscr{R}$ in the following. Any functioning regime is conveniently represented in terms of limiting and intermediate solutions. We formally define as intermediate a solution whose qualitative structure remains unaltered under arbitrary small variations of the ambient pressure. Conversely, a solution is a limiting one if an arbitrary small variation of the ambient pressure produces modifications to its qualitative structure, that is, limiting solutions are isolated solutions of the boundary value problem. Correspondingly, a set of limiting values of the ambient pressure is defined; each pressure value is associated with a limiting flow. Intermediate solutions are observed whenever the ambient pressure lies between two consecutive limiting values. Generally speaking, the qualitative structure of a solution is characterized by the existence and the possible sequence of shock waves. This will be made clear in the subsequent discussion.

It is anticipated here, for the understanding of the following treatment, that starting from five different isentropic patterns associated with the reservoir conditions, as many as 10 different functioning regimes have been singled out in the present analysis, and they are gathered in the six classes in table 2. Two classical functioning regimes are introduced: the ideal one $\mathscr{R}^{I}$ in § 3.2 and the non-ideal one $\mathscr{R}^{NI}$ in § 3.7, which are produced by reservoir conditions of type $\mathscr{S}^{I}$ and $\mathscr{S}^{NI}$, respectively. These two

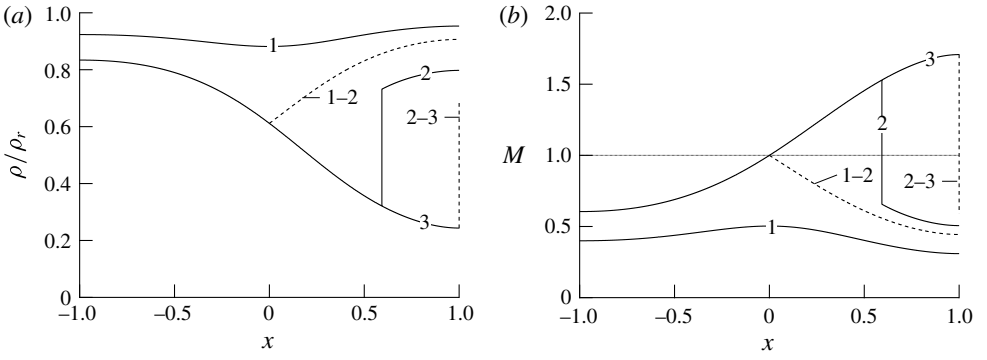

FIGURE 5. Exemplary limiting (- - - -) and intermediate (——) flows of type $\mathscr{R}^I$, computed from the van der Waals polytropic model with $c_v/R = 50$. (*a*) Density solutions, scaled to reservoir density ρ_r; (*b*) Mach number solutions. Reservoir conditions: $P_r = 10P_c$, $v_r = 10v_c$.

regimes are characterized by the possibility of observing a classical compression shock in the divergent section. Regime $\mathscr{S}^{NI}$ further allows for a non-monotone evolution of the Mach number in the supersonic divergent section. Reservoir conditions featuring pattern $\mathscr{S}_3^{NC}$ produce the non-classical regime $\mathscr{R}_3^{NC}$ described in § 3.3, which features non-monotonic Mach number profile in the subsonic regime, in both the converging and diverging sections. As for non-classical functioning regimes associated with patterns $\mathscr{S}_1^{NC}$ and $\mathscr{S}_2^{NC}$, two general classes may be delineated, namely $\mathscr{R}_1^{NC}$ and $\mathscr{R}_2^{NC}$, both possibly featuring rarefaction shocks. In the case of the $\mathscr{R}_2^{NC}$ flows detailed in § 3.4, the rarefaction shock is sonic on the upstream side and it is located in the converging section of the nozzle. In flows of type $\mathscr{R}_1^{NC}$, the rarefaction shock is sonic on the downstream side and it lies in the diverging section of the nozzle, see § 3.5. A further grouping is outlined, that is sub-classes *a*, *b* and *c* of $\mathscr{R}_1^{NC}$ and $\mathscr{R}_2^{NC}$, which are defined in § 3.6 according to the occurrence of shock splitting. Finally, it is shown in § 3.8 that a non-classical functioning regime, namely $\mathscr{R}_0^{NC}$, is produced by $\mathscr{S}^{NI}$ reservoir conditions which are characterized by the occurrence of a single sonic point.

Functioning regimes will be discussed in the order of increasing number of possible transition of the isentropic pattern (see the ordering in (2.10)), starting from $\mathscr{S}^I$ reservoir conditions, where no transition can take place, up to $\mathscr{S}^{NI}$ reservoir conditions, from where all transitions are possible.

3.2. *Functioning regime* $\mathscr{R}^I$

The layout of the possible flow configurations produced by $\mathscr{S}^I$ reservoir conditions corresponds to the textbook case of an ideal gas with constant specific heats, see for instance Thompson (1988). The main results are reported here for reference and are extended to a general, non-ideal thermodynamic description of the fluid. Limiting and intermediate flows are reported in figure 5. Flows of type $\mathscr{R}^I(1)$ are completely subsonic and are characterized by increasing mass flow rate with decreasing ambient pressure. Limiting solution $\mathscr{R}^I(1\text{–}2)$ determines the so-called choking condition, because the throat is sonic and a further decrease of the ambient pressure has no influence on the mass flow rate. Let $\dot{m}_{max}$ denote the maximum mass flow rate

dischargeable by the nozzle and $\dot{m}_s$ the mass flow rate in the choked condition; then

$$\dot{m}_{max} = \dot{m}_s = \dot{m}_c(s_r, h^t), \tag{3.1}$$

where the critical mass flow rate $\dot{m}_c$ is defined by (2.7) and s_r is the reservoir entropy. If $\beta < \beta_{1\text{–}2}$, where $\beta_{1\text{–}2}$ is the pressure ratio corresponding to limiting solution $\mathscr{R}^I(1\text{–}2)$, the flow is choked and subsonic to supersonic transition occurs at the throat. Intermediate flows $\mathscr{R}^I(2)$ include a compression shock wave in the diverging section of the nozzle. It can be shown that the entropy jump across the shock wave increases with decreasing ambient pressure. The mass balance equation, evaluated on the outlet section, provides an implicit definition for $s_e(P_e; \dot{m}, h^t, A_e)$, where subscript e denotes the exit quantities. Thus, if the flow is choked, we obtain

$$\frac{\mathrm{d}s_e}{\mathrm{d}P_e} = \frac{M_e^2 - 1}{\rho_e T_e (M_e^2 G_e + 1)}. \tag{3.2}$$

Note that if the outflow is subsonic, as is the case for solutions of type $\mathscr{R}^I(2)$, then $P_e = P_a$ and $\mathrm{d}s_e/\mathrm{d}P_e = \mathrm{d}s_e/\mathrm{d}P_a$ in the corresponding range of β. In addition, by combining the jump relations and the differential relations for quasi-1D flows, one has

$$\frac{\mathrm{d}x_s}{\mathrm{d}s_B} = \frac{A}{A'} \frac{\rho_A T_B}{[P]} \left(\frac{1}{M_B^2} + \frac{[v]}{2v_B} G_B \right) \left[\left(\frac{1}{M_B^2} - 1 \right) \frac{v_B}{v_A} + \frac{1}{2} \right]^{-1}, \tag{3.3}$$

where x_s is the location of the shock wave and $[X] = X_B - X_A$ is the jump between a quantity evaluated at the post-shock state (subscript B) and at the pre-shock state (subscript A). Given that $M_B < 1$, the last two terms are positive (the condition $2v_B + [v]G_B = 0$ is the singularity that limits the maximum possible density increase across compression shocks, see Kluwick 2001). Hence, a compression shock in the diverging section of the nozzle moves downstream with increasing post-shock entropy, which, in turn, corresponds to decreasing values of the ambient pressure, as is seen by (3.2) together with $s_e = s_B$ and $P_e = P_a$. Ultimately, the shock wave reaches the exit section, see limiting flow $\mathscr{R}^I(2\text{–}3)$. Flows of type $\mathscr{R}^I(3)$ have supersonic exit conditions and may exhibit an over-expanded or under-expanded jet outside of the nozzle if $\beta \neq \beta_3$, where β_3 corresponds to the exit pressure of solution $\mathscr{R}^I(3)$.

3.3. *Functioning regime* $\mathscr{R}_3^{NC}$

If the reservoir conditions correspond to isentropic pattern $\mathscr{S}_3^{NC}$, the Mach number does not increase monotonically through a subsonic expansion. The related functioning regime is a non-classical one, since $J > 0$ in a subsonic flow requires $\Gamma < 0$, and it is denoted by $\mathscr{R}_3^{NC}$. Limiting and intermediate flows of regime $\mathscr{R}_3^{NC}$ are sketched in figure 6. The layout and the general properties of the solutions are as described above for the case $\mathscr{R}^I$, except for a pronounced subsonic peak in the Mach number. This appears as a steeper expansion or compression in the density solutions. In addition, contrary to the ideal case, in flows of type $\mathscr{R}_3^{NC}(2)$ the Mach number may also increase downstream of the shock wave in the divergent section. If, however, transition $\mathscr{S}_2^{NI} \to \mathscr{S}^I$ occurs in passing through the shock wave, the Mach number will necessarily decrease up to the exit section, as in the exemplary solution $\mathscr{R}_3^{NC}(2)$ reported in figure 6.

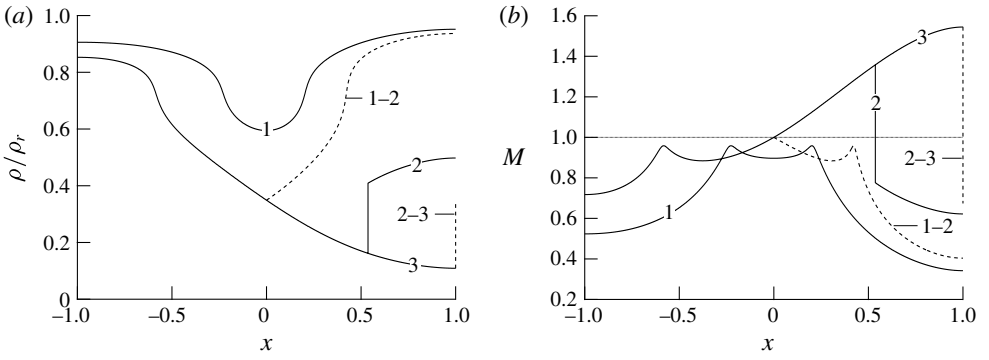

FIGURE 6. Exemplary limiting (- - - -) and intermediate (——) flows of type $\mathscr{R}_3^{NC}$, computed from the van der Waals polytropic model with $c_v/R = 50$. (*a*) Density solutions, scaled to reservoir density ρ_r; (*b*) Mach number solutions. Reservoir conditions: $P_r = 1.1427P_c,\ v_r = 0.8058v_c$.

3.4. *Functioning regimes* $\mathscr{R}_2^{NC}$

When the isentropic pattern of the reservoir conditions exhibits three sonic points, the layout of the possible flow fields is considerably more complex. Here we discuss regimes of type $\mathscr{R}_2^{NC}$, which exhibit a rarefaction shock wave in the converging section of the nozzle and can originate from reservoir conditions of type $\mathscr{S}_2^{NC}$, see table 2. Three possible configurations are admissible and detailed in § 3.6: $\mathscr{R}_{2a}^{NC}$, $\mathscr{R}_{2b}^{NC}$ and $\mathscr{R}_{2c}^{NC}$. Here, the regime $\mathscr{R}_{2a}^{NC}$ in figure 7 – corresponding to the Type-2 flows of Cramer & Fry (1993) – is presented to describe common features to all $\mathscr{R}_2^{NC}$ regimes.

Inspection of figure 7 reveals that flows such as $\mathscr{R}_{2a}^{NC}(2)$, including a single compression shock in the diverging section of the nozzle, exist for a very limited range of ambient pressure. This shock, owing to the non-monotone dependence of the Mach number on the density, ultimately has sonic upstream state ($\rho = \rho_{s_2}$), see limiting solution $\mathscr{R}_{2a}^{NC}(2\text{–}3)$, and cannot exist further downstream. Shocks with upstream sonic state will be referred to as pre-sonic shocks in the following.

If the ambient pressure is slightly reduced below $\beta = \beta_{2\text{–}3}$, the necessary entropy rise is carried by a double-shock configuration, in which the leading wave is a rarefaction shock and the trailing wave is a pre-sonic compression shock. The trailing shock is formed because the flow downstream of the rarefaction shock becomes sonic when $\rho = \rho_{s_2}$ in the local isentropic pattern, which remains of type $\mathscr{S}_2^{NC}$ (i.e. no transition occurs across the leading shock). Intermediate flows of type $\mathscr{R}_{2a}^{NC}(2)$ and $\mathscr{R}_{2a}^{NC}(3)$ are sonic at the throat (sonic condition ρ_{s_1}). Therefore, the nozzle is choked in the corresponding range of ambient pressure, with a constant value of the mass flow rate denoted as $\dot{m}_{s_1}$. Moreover, the simultaneous shift upstream of the rarefaction shock and downstream of the pre-sonic compression shock, in accordance with relation (3.3), makes it possible to satisfy the overall increasing entropy jump in a choked flow as the ambient pressure is decreased, cf. (3.2). Eventually, the leading shock wave has sonic upstream state and it is located exactly at the throat section, see limiting solution $\mathscr{R}_{2a}^{NC}(3\text{–}4)$.

A rarefaction shock with sonic upstream state can also exist ahead of the throat. If $\beta_{4\text{–}5} < \beta < \beta_{3\text{–}4}$, the mass flow rate increases with decreasing ambient pressure and sonic condition ρ_{s_1} occurs upstream of the throat. Trajectories such as $\mathscr{R}_{2a}^{NC}(4)$ can be continued provided a sonic rarefaction shock is inserted at the sonic point. Notably,

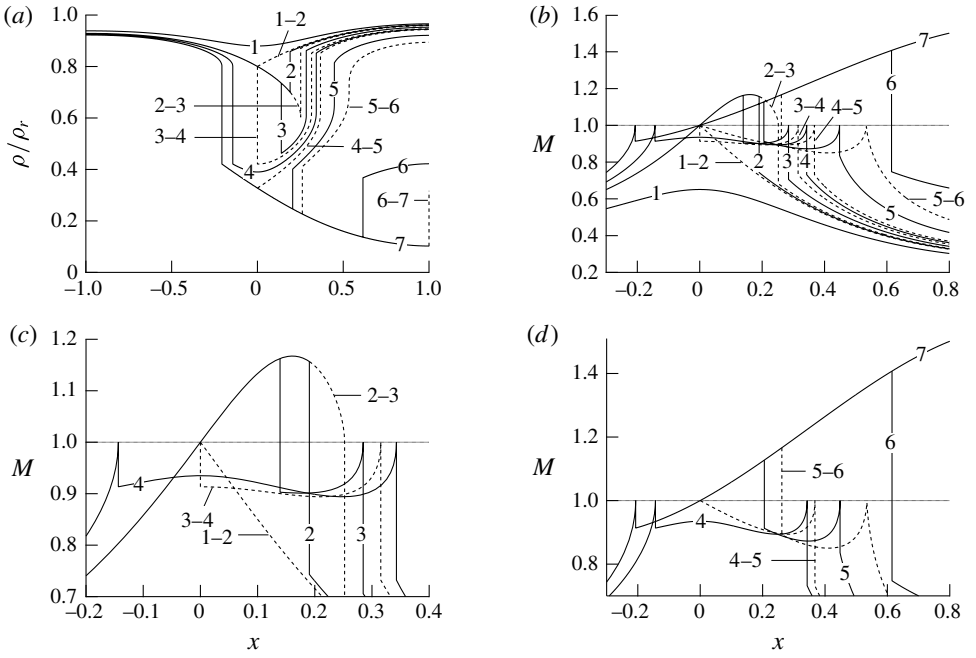

FIGURE 7. Exemplary limiting (- - - -) and intermediate (——) flows of type $\mathscr{R}_{2a}^{NC}$, computed from the van der Waals polytropic model with $c_v/R = 50$. (*a*) Density solutions, scaled to reservoir density ρ_r; (*b*) Mach number solutions; (*c*) enlargement of (*b*) including only flows from 2 to 4; (*d*) enlargement of (*b*) including only flows from 4 to 7. Reservoir conditions: $P_r = 1.1300P_c,\ v_r = 0.7710v_c$.

this shock has the same upstream and downstream states as the leading shock in limiting flow $\mathscr{R}_{2a}^{NC}(3\text{–}4)$, albeit in a different location. Downstream of the rarefaction shock, the flow expands up to the throat because of the converging area. Flows of type $\mathscr{R}_{2a}^{NC}(4)$ are subsonic at the throat and therefore the pressure and density increase in the diverging section of the nozzle. Because the local isentropic pattern is $\mathscr{S}_2^{NC}$, a pre-sonic compression shock must be inserted to continue the flow beyond sonic point ρ_{s_2} (this shock is identical to that of limiting solution $\mathscr{R}_{2a}^{NC}(3\text{–}4)$). The mass flow rate can be increased by decreasing β until $M = 1$ at the throat, whereby the sonic condition corresponds to the low-density sonic point ρ_{s_3} in the isentrope downstream of the rarefaction shock. This condition determines limiting flow $\mathscr{R}_{2a}^{NC}(4\text{–}5)$, in which the pre-sonic rarefaction shock is in its rearmost position. Let s_t denote the entropy value downstream of this shock wave and let $\dot{m}_{s_2}$ be the mass flow rate corresponding to $\beta = \beta_{4\text{–}5}$. Then

$$\dot{m}_{max} = \dot{m}_{s_2} = \dot{m}_c(s_t, h^t) < \dot{m}_c(s_r, h^t), \tag{3.4}$$

where the last inequality follows from $(\partial j/\partial s)_{\rho,h^t} = -\rho T(1+G)/\sqrt{2(h^t - h)}$, which gives $(\partial \dot{m}_c/\partial s)_{h^t} < 0$ and from the admissibility requirement $s_t > s_r$. Note that there exist two different choking conditions in functioning regime $\mathscr{R}_{2a}^{NC}$, namely $\beta_{3\text{–}4} < \beta < \beta_{1\text{–}2}$ $(\dot{m} = \dot{m}_{s_1})$ and $\beta < \beta_{4\text{–}5}$ $(\dot{m} = \dot{m}_{s_2})$.

Flows such as $\mathscr{R}_{2a}^{NC}(5)$ or $\mathscr{R}_{2a}^{NC}(6)$ admit ordinary compression shock waves in the diverging section of the nozzle. If the shock is sufficiently close to the throat, as in

case $\mathscr{R}^{NC}_{2a}(5)$, the resultant subsonic compression eventually attains a sonic point and a further shock, with sonic upstream state, must be formed to continue the flow. Following Kluwick (1993) and Cramer & Fry (1993), we will refer to this double compression-shock configuration as a split shock, owing to the analogies with the shock-splitting phenomenon in unsteady flows (see Wendroff 1972; Menikoff & Plohr 1989; Cramer 1991). According to relation (3.3), if the leading compression shock moves downstream the corresponding entropy jump increases. Indeed, a reduction of the ambient pressure results in a stronger leading shock and in a weaker terminating shock. Ultimately, the entropy rise across the first compression shock is such that, in the downstream flow, the isentropic pattern corresponds to the transitional type $\mathscr{S}^{NC}_2/\mathscr{S}^{NC}_3$. Thus, in the limiting flow $\mathscr{R}^{NC}_{2a}(5\text{–}6)$ the trailing sonic shock wave has vanishing strength.

If $\beta < \beta_{5\text{–}6}$, a single non-sonic compression shock occurs, because the post-shock isentropic pattern is either $\mathscr{S}^{NC}_3$ or $\mathscr{S}^{I}$. Hence, if a compression shock forms sufficiently far downstream of the throat, as is the case in flows of type $\mathscr{R}^{NC}_{2a}(6)$, the post-shock isentrope no longer contains the sonic point required for the existence of the sonic compression shock. As in previous regimes, with decreasing ambient pressure the shock wave moves downstream in the diverging section of the nozzle and eventually attains the exit section in limiting flow $\mathscr{R}^{NC}_{2a}(6\text{–}7)$. If $\beta < \beta_{6\text{–}7}$, no shock waves exist downstream of the throat and the outflow is supersonic. The major difference with respect to flows including a single sonic point is that flows such as $\mathscr{R}^{NC}_{2a}(7)$, having arbitrarily large exit Mach number, must include a pre-sonic rarefaction shock upstream of the throat.

3.5. *Functioning regimes* $\mathscr{R}^{NC}_1$

Regimes of type $\mathscr{R}^{NC}_1$, including regimes $\mathscr{R}^{NC}_{1a}$, $\mathscr{R}^{NC}_{1b}$ and $\mathscr{R}^{NC}_{1c}$ described in § 3.6, exhibit a rarefaction shock wave in the diverging section of the nozzle and can originate from reservoir conditions of type $\mathscr{S}^{NC}_1$ or $\mathscr{S}^{NC}_2$, see table 2. The regime $\mathscr{R}^{NC}_{1a}$ in figure 8 – corresponding to Type-1 flows of Cramer & Fry (1993) – is now presented to outline all regimes of type $\mathscr{R}^{NC}_1$.

With reference to figure 8, flows $\mathscr{R}^{NC}_{1a}(1)$, $\mathscr{R}^{NC}_{1a}(2)$ and $\mathscr{R}^{NC}_{1a}(3)$ are qualitatively similar to $\mathscr{R}^{NC}_{2a}(1)$, $\mathscr{R}^{NC}_{2a}(2)$ and $\mathscr{R}^{NC}_{2a}(3)$, respectively, discussed in the previous section. Differently from $\mathscr{R}^{NC}_{2a}(3)$, the rarefaction shock of intermediate flow $\mathscr{R}^{NC}_{1a}(3)$ becomes sonic on the downstream side (post-sonic shock) when $\beta = \beta_{3\text{–}4}$. Rarefaction shocks cannot exist ahead of this limiting sonic shock. Thus, in contrast to $\mathscr{R}^{NC}_{2a}$ flows, functioning regime $\mathscr{R}^{NC}_{1a}$ exhibits a unique sonic condition at the throat, corresponding to the high-density sonic point ρ_{s1}. Accordingly,

$$\dot{m}_{max} = \dot{m}_s = \dot{m}_c(s_r, h^t), \tag{3.5}$$

where $\dot{m}_s$ is the mass flow rate discharged when $\beta < \beta_{1\text{–}2}$. If $\beta < \beta_{3\text{–}4}$, the flow expands downstream of the limiting rarefaction shock and two different shock configurations are possible, similarly to functioning regime $\mathscr{R}^{NC}_{2a}$. Compression waves in the neighbourhood of the limiting rarefaction shock occur in the form of a split shock, see intermediate flow $\mathscr{R}^{NC}_{1a}(4)$. The split-shock configuration ultimately vanishes because of the disintegration of the sonic compression shock, as a result of the shift in the isentrope across the leading compression shock. If $\beta_{5\text{–}6} < \beta < \beta_{4\text{–}5}$, a single non-sonic shock is formed downstream of the limiting rarefaction shock, for the subsequent flow remains subsonic. Finally, flows such as $\mathscr{R}^{NC}_{1a}(6)$, expanding to

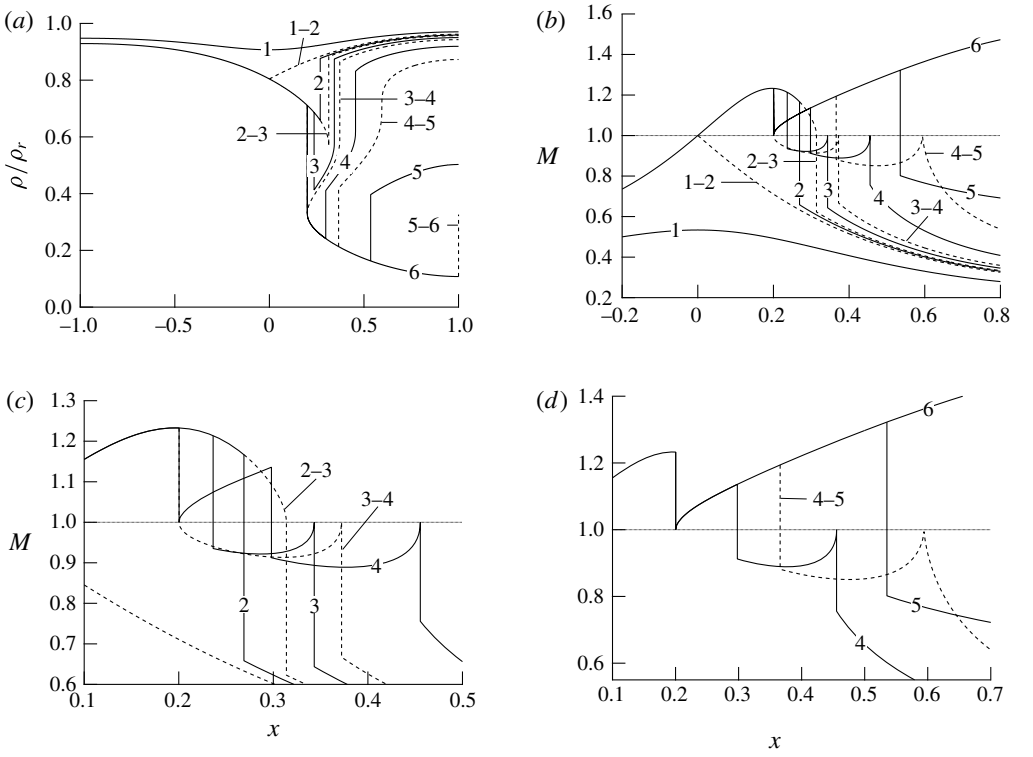

FIGURE 8. Exemplary limiting (- - - -) and intermediate (——) flows of type $\mathscr{R}^{NC}_{1a}$, computed from the van der Waals polytropic model with $c_v/R = 50$. (*a*) Density solutions, scaled to reservoir density ρ_r; (*b*) Mach number solutions; (*c*) enlargement of (*b*) including only flows from 2 to 4; (*d*) enlargement of (*b*) including only flows from 4 to 6. Reservoir conditions: $P_r = 1.1453P_c$, $v_r = 0.7600v_c$.

arbitrarily low densities and arbitrarily large Mach numbers, are realizable provided that a rarefaction shock with sonic downstream state is inserted into the diverging section of the nozzle.

The two non-classical functioning regimes that we have described so far, namely $\mathscr{R}^{NC}_{1a}$ and $\mathscr{R}^{NC}_{2a}$, are in fact the Type-1 and Type-2 flows introduced by Cramer & Fry (1993), respectively, and have been introduced to describe the features of $\mathscr{R}^{NC}_{1}$ and $\mathscr{R}^{NC}_{2}$ flows, respectively. In the following section we show that a further classification can be formulated according to the mechanism by which the split shock turns into the single-shock configuration.

3.6. *On the split-shock/single-shock transition: sub-classes $\mathscr{R}^{NC}_{a}$, $\mathscr{R}^{NC}_{b}$ and $\mathscr{R}^{NC}_{c}$*

In order to investigate the different scenarios for the split-shock formation and eventual disintegration, it is instructive to examine the quantity

$$\Psi = j(\rho; s, h^t) - j^*(\rho; s), \tag{3.6}$$

where j^* is the mass flux corresponding to a post-sonic compression shock, which is the difference between the slopes of the Rayleigh lines for a shock with total enthalpy h^t and for a post-sonic compression shock, both centred on the thermodynamic state

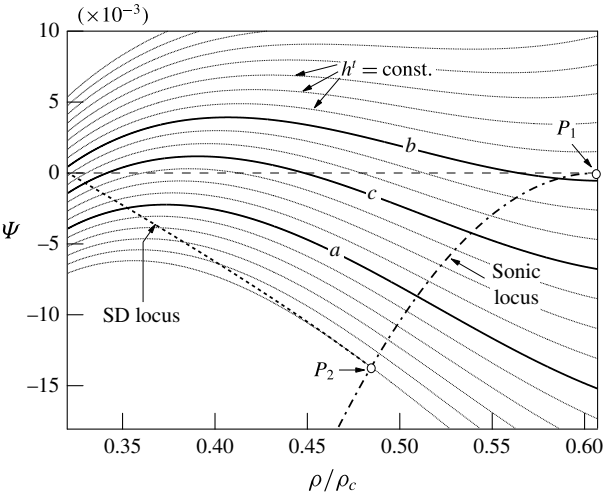

FIGURE 9. Isolines of h^t in the Ψ–ρ diagram corresponding to the exemplary isentrope $s = s(1.0923P_c, v_c)$, as computed from the van der Waals polytropic model with $c_v/R = 50$. The range of densities is restricted to those where j^* is defined, i.e. where a post-sonic compression shock can possibly originate. Two additional curves are plotted: the sonic locus $M = 1$ and the sonic shock disintegration (SD) locus, gathering the pre-shock states corresponding to a shock wave with downstream isentropic pattern $\mathscr{S}_2^{NC}/\mathscr{S}_3^{NC}$. The SD locus intersects the sonic locus at point P_2. The curve passing through point P_2 corresponds to the transitional isentropic pattern $\mathscr{S}_2^{NC}/\mathscr{S}_3^{NC}$. On the other hand, the curve passing through point P_1 ($M = 1$ and $\Psi = 0$) corresponds to the transitional isentropic pattern $\mathscr{S}^{NI}/\mathscr{S}_1^{NC}$.

identified by ρ and s. Note that j^* and, in turn, Ψ are defined only if a post-sonic compression shock can originate from the given pre-shock state. By analysing the properties of non-convex shock adiabats, it is possible to prove (see e.g. Kluwick 2001) that, if a post-sonic compression shock centred on a given pre-shock state exists and is admissible, then it is unique.

Figure 9 shows exemplary isolines of h^t in the Ψ–ρ plane of a given isentrope. In this diagram, the abscissa spans the range of densities where a post-sonic compression shock is admissible. Two relevant curves are plotted, namely the sonic locus and the sonic shock disintegration (SD) locus. States located at densities lower than those on the sonic locus represent supersonic, and therefore candidate pre-shock states of admissible shock waves. By combining (3.3) with the well-known differential relations for quasi-1D isentropic flows, it is easy to show that the entropy jump increases with decreasing density of the candidate pre-shock state, provided that the shock wave is compressive. Ultimately, when the pre-shock state occurs on the SD locus, the post-shock isentropic pattern corresponds to the transitional type $\mathscr{S}_2^{NC}/\mathscr{S}_3^{NC}$.

To aid understanding of the following analysis, the possible compression-wave configurations in the thermodynamic region of interest in this work have been sketched in the P–v plane, see figure 10. Here ρ_A denotes the density at the selected pre-shock state A and ρ_{SD} represents the density corresponding to the intersection between $\Psi(\rho; s, h^t)$ and the SD locus. Split shocks occur when $\Psi < 0$ and $\rho_A > \rho_{SD}$, because, along the isentropic compression resulting from shock A–B, sonic point S

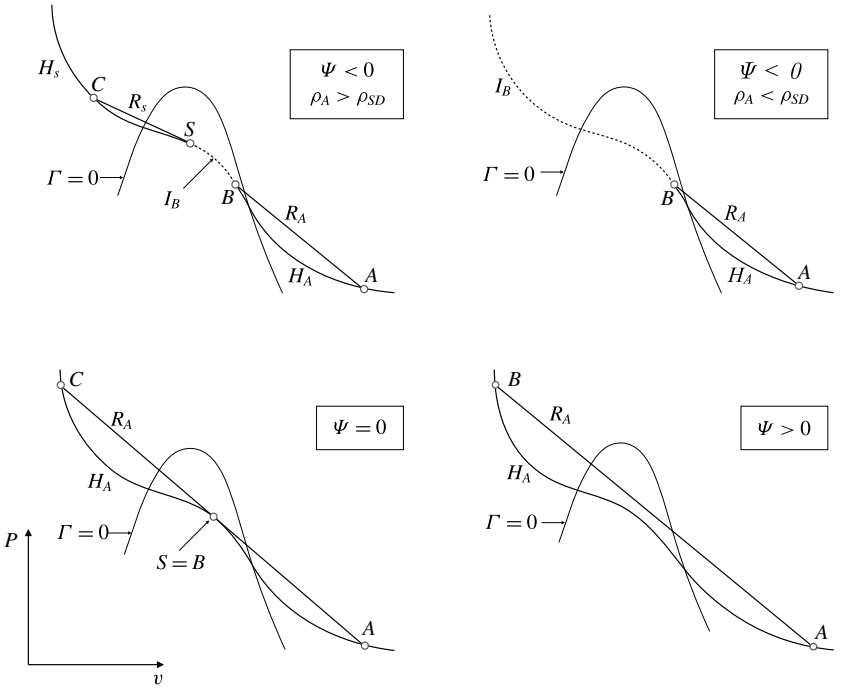

FIGURE 10. Qualitative chart illustrating compression waves that bridge the negative-Γ region: H_A and H_S are shock adiabats from points A and S, respectively; R_A and R_S are Rayleigh lines; I_B is an isentrope. Case $\Psi < 0$, $\rho_A > \rho_{SD}$: split-shock composed of shock A–B, isentropic compression along I_B up to sonic point S and sonic shock S–C. Case $\Psi < 0$, $\rho_A < \rho_{SD}$: shock A–B followed by isentropic compression along I_B. Case $\Psi = 0$: the Rayleigh line R_A of shock A–C is tangent to the shock adiabat H_A at the intermediate sonic step S; this shock can be seen as a unique non-sonic shock or as the composition of post-sonic shock A–S and pre-sonic shock S–C. Case $\Psi > 0$: single shock A–B; the Rayleigh line R_A bridges the concave-down region of H_A.

is encountered and a further shock wave is required to continue the flow. Note that state S is necessarily embedded in the region $\Gamma < 0$, for the curvatures of the shock adiabat and of the isentrope have the same sign in the P–v plane at a sonic point (see, e.g. Menikoff & Plohr 1989).

There exist two different mechanisms by which the split shock turns into an ordinary non-sonic shock. In the first case, the transition takes place when state A crosses the SD locus and the sonic shock disintegrates. As a result, if $\Psi < 0$ and $\rho_A < \rho_{SD}$, sonic point S is no longer encountered in the isentropic compression downstream of shock A–B. The split-shock/single-shock transition is also accomplished when Ψ changes sign. As Ψ goes to zero from below, a weaker isentropic compression and a stronger terminating shock are generated. When $\Psi = 0$, state B and sonic point S coincide, i.e. the intermediate isentropic compression vanishes. In this case, the leading shock A–B and the trailing shock S–C merge in the single large-amplitude shock A–C. If $\Psi > 0$ an ordinary shock occurs, because the Rayleigh line completely bridges, without touching, the region where the shock adiabat H_A is concave down (inflection points of the shock adiabat nearly coincide with the intersections between the shock adiabat and the $\Gamma = 0$ locus, see for instance Kluwick 2001).

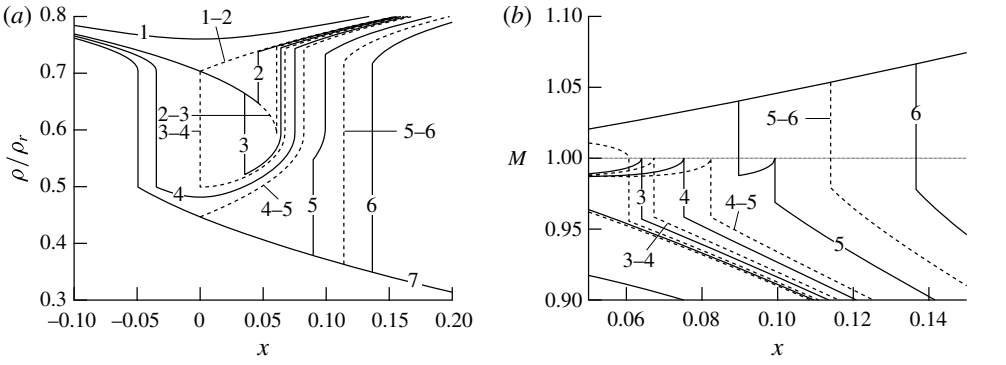

FIGURE 11. Exemplary limiting (- - - -) and intermediate (——) flows of type $\mathscr{R}^{NC}_{2b}$, computed from the van der Waals polytropic model with $c_v/R = 50$. (*a*) Density solutions, scaled to reservoir density ρ_r; (*b*) Mach number solutions. Reservoir conditions: $P_r = 1.2824P_c,\ v_r = 0.7863v_c$.

We now examine the different configuration reported in figure 9. Curves such as *a* display $\Psi < 0$; the split-shock configuration is formed and eventually vanishes when the pre-shock state crosses the SD locus. We will refer to functioning regimes featuring this kind of split-shock/single-shock transition as the sub-class $\mathscr{R}^{NC}_{a}$, which includes $\mathscr{R}^{NC}_{1a}$ and $\mathscr{R}^{NC}_{2a}$. The curve labelled *b* in figure 9 exhibits a zero with $\mathrm{d}\Psi/\mathrm{d}\rho < 0$. In this case, by decreasing the pre-shock density, the two compression shocks in the split-shock configuration merge in a single large-amplitude shock. We will refer to functioning regimes featuring this kind of split-shock/single-shock transition as the sub-class $\mathscr{R}^{NC}_{b}$ ($\mathscr{R}^{NC}_{1b}$ and $\mathscr{R}^{NC}_{2b}$). Figure 11 reports the layout of limiting and intermediate flows corresponding to the exemplary case $\mathscr{R}^{NC}_{2b}$. The limiting flow corresponding to the overlapping of the compression shocks is $\mathscr{R}^{NC}_{2b}$(5–6). It is noticeable that the split-shock/single-shock transition of $\mathscr{R}^{NC}_{b}$ regimes is qualitatively similar to the transition predicted by the isentropic theory, i.e. if we were to neglect the entropy rise across shock waves (see Cramer & Fry 1993; Kluwick 1993).

In addition to $\mathscr{R}^{NC}_{a}$ and $\mathscr{R}^{NC}_{b}$ sub-classes, we introduce the sub-class $\mathscr{R}^{NC}_{c}$ ($\mathscr{R}^{NC}_{1c}$ and $\mathscr{R}^{NC}_{2c}$) of the functioning regimes in which a double split-shock/single-shock transition occurs. This is expected when the stagnation conditions are such that Ψ has two zeros, as is the case in curves of type *c* in figure 9. The layout of the limiting and intermediate flows for the exemplary case $\mathscr{R}^{NC}_{1c}$ is sketched in figure 12. When the high-density zero of Ψ ($\mathrm{d}\Psi/\mathrm{d}\rho < 0$) is encountered, the two compression shocks merge, see limiting flow $\mathscr{R}^{NC}_{1c}$(4–5). The reverse process occurs in limiting solution $\mathscr{R}^{NC}_{1c}$(5–6), because the pre-shock density corresponds to the low-density zero of Ψ, where $\mathrm{d}\Psi/\mathrm{d}\rho > 0$. By further decreasing the pre-shock density, the split shock ultimately vanishes as in $\mathscr{R}^{NC}_{a}$ regimes, i.e. the sonic shock disintegrates.

3.7. *Functioning regime* $\mathscr{R}^{NI}$

The layout of the possible flows corresponding to reservoir conditions of type $\mathscr{S}^{NI}$ depends on the possible shock-induced transitions of the isentropic pattern. First of all, note that rarefaction shocks cannot occur in these flows, as in any other functioning regime produced by reservoir conditions featuring a unique sonic point.

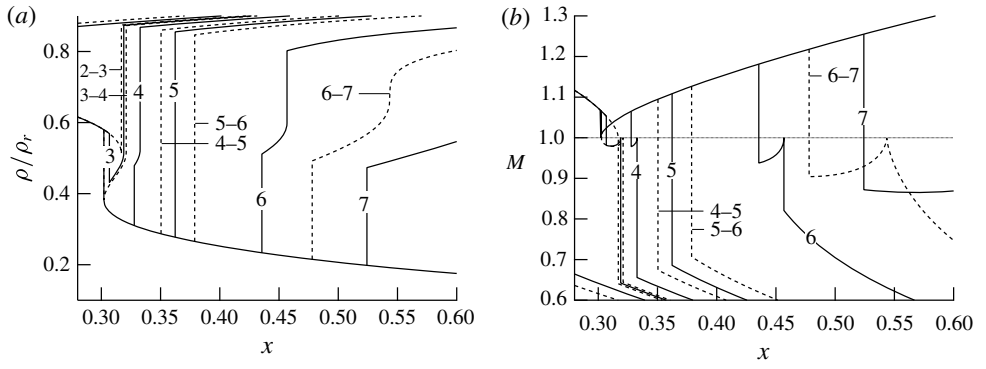

FIGURE 12. Exemplary limiting (- - - -) and intermediate (——) flows of type $\mathscr{R}^{NC}_{1c}$, computed from the van der Waals polytropic model with $c_v/R = 50$. (*a*) Density solutions, scaled to reservoir density ρ_r; (*b*) Mach number solutions. Reservoir conditions: $P_r = 1.2102P_c,\ v_r = 0.7542v_c$.

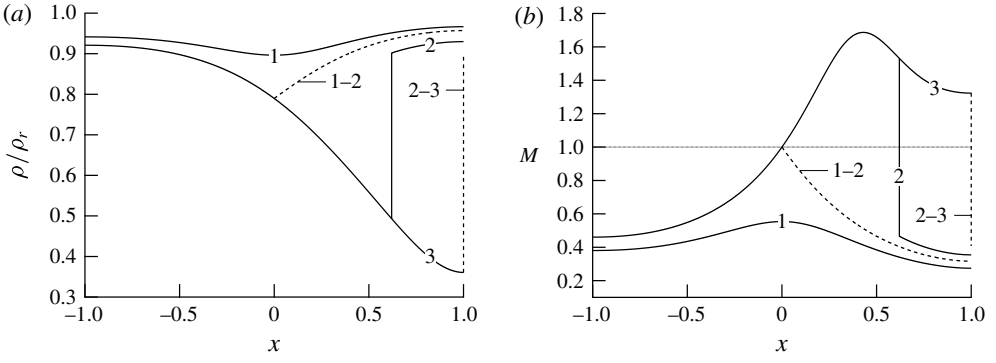

FIGURE 13. Exemplary limiting (- - - -) and intermediate (——) flows of type $\mathscr{R}^{NI}$, computed from the van der Waals polytropic model with $c_v/R = 50$. (*a*) Density solutions, scaled to reservoir density ρ_r; (*b*) Mach number solutions. Reservoir conditions: $P_r = 1.7355P_c,\ v_r = 0.6532v_c$.

This is easily seen by analysing the related mass flux functions or phase planes. However, compression waves near the negative-Γ region may occur either as ordinary non-sonic shocks or in the form of split shocks, according to the slope of the Rayleigh line. The same argument concerning the Ψ–ρ diagram could be repeated for this type of nozzle flow. The functioning regime arising from reservoir conditions of type $\mathscr{S}^{NI}$ and corresponding to the case $\Psi > 0$, which implies that compression shocks occurring in the diverging section of the nozzle are ordinary non-sonic shocks, is denoted as $\mathscr{R}^{NI}$. In other words, the possible shock-induced transition of the isentropic pattern does not determine any limiting solutions, so that the layout of limiting and intermediate flows is as shown in figure 13. This functioning regime stands out from $\mathscr{R}^{I}$ and $\mathscr{R}^{NC}_{3}$ (which have qualitatively similar density solutions) because the Mach number is non-monotone along supersonic branches of isentropic expansions. Moreover, $\mathscr{R}^{NI}$ is referred to as a non-ideal regime, rather than a non-classical one, because it requires the less restrictive condition $\Gamma < 1$.

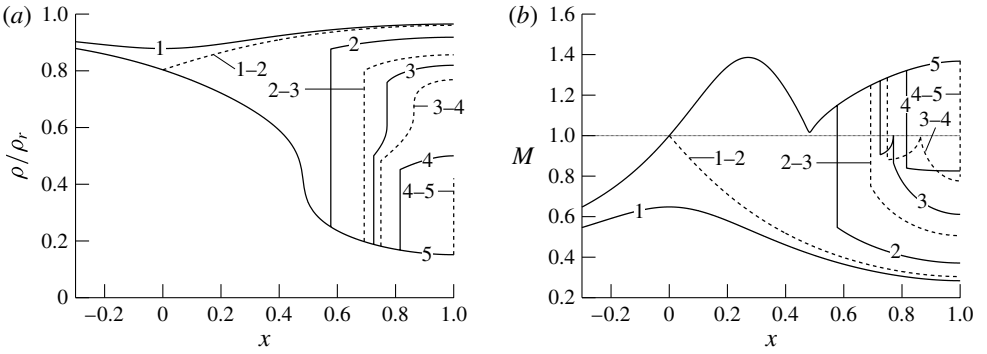

FIGURE 14. Exemplary limiting (- - - -) and intermediate (——) flows of type $\mathscr{R}_0^{NC}$, computed from the van der Waals polytropic model with $c_v/R = 50$. (*a*) Density solutions, scaled to reservoir density ρ_r; (*b*) Mach number solutions. Reservoir conditions: $P_r = 1.2315P_c,\ v_r = 0.7287v_c$.

3.8. *Functioning regime* $\mathscr{R}_0^{NC}$

To conclude, we present one additional functioning regime, namely $\mathscr{R}_0^{NC}$, which develops from reservoir states associated with the isentropic pattern $\mathscr{S}^{NI}$. Following previous discussion, shocks that bridge the negative-Γ region are expected to split if the isentropic pattern downstream of a generic non-sonic shock exhibits three sonic points and the post-shock state lies between sonic points ρ_{s3} and ρ_{s2}. In this case, the resultant subsonic compression eventually encounters sonic point ρ_{s2} and a further shock is required. The layout of limiting and intermediate flows of the type $\mathscr{R}_0^{NC}$ is depicted in figure 14. The splitting mechanism in limiting solution $\mathscr{R}_0^{NC}(2\text{–}3)$ is the same occurring in $\mathscr{R}_c^{NC}$ regimes when the low-density zero of Ψ $(\mathrm{d}\Psi/\mathrm{d}\rho > 0)$ is crossed. Similarly to regimes of type $\mathscr{R}_a^{NC}$, a decrease in ambient pressure results in a weaker sonic shock, which ultimately vanishes when $\beta = \beta_{3\text{–}4}$.

It is remarkable that past qualitative investigations of nozzle flows, based on the simplifying assumption of isentropic flow, i.e. neglecting the entropy rise and the resultant shift in the isentropes across shock waves, led to the erroneous conclusion that non-classical nozzle flows develop exclusively from reservoir states featuring three sonic points.

4. Thermodynamic map of functioning regimes

In this section, we formalize the connection between the functioning regimes and the reservoir conditions, which was anticipated in § 3.1. Figure 15 reports a thermodynamic map (in the P–v diagram) of the reservoir states leading to each functioning regime described in §§ 3.2–3.8. Firstly, if the isentropic pattern of the reservoir condition is $\mathscr{S}^{I}$, then the only possible functioning regime is $\mathscr{R}^{I}$. Indeed, starting from pattern $\mathscr{S}^{I}$, a possible entropy rise across shock waves cannot modify the isentropic pattern, see ordering relation (2.10). If $0 < \Gamma < 1$ somewhere along the reservoir isentrope (for $s_r > s_{vle}$), $\mathscr{R}^{NI}$ is possible in addition to $\mathscr{R}^{I}$. The transition between said functioning regimes corresponds to the transition between reservoir pattern $\mathscr{S}^{NI}$, leading to regime $\mathscr{R}^{NI}$ in the thermodynamic region considered, and reservoir pattern $\mathscr{S}^{I}$, leading to $\mathscr{R}^{I}$. Therefore, the transition boundary $\mathscr{S}^{NI}/\mathscr{S}^{I}$ in figure 3 is coincident with the boundary $\mathscr{R}^{NI}/\mathscr{R}^{I}$ in figure 15. This, again, is because

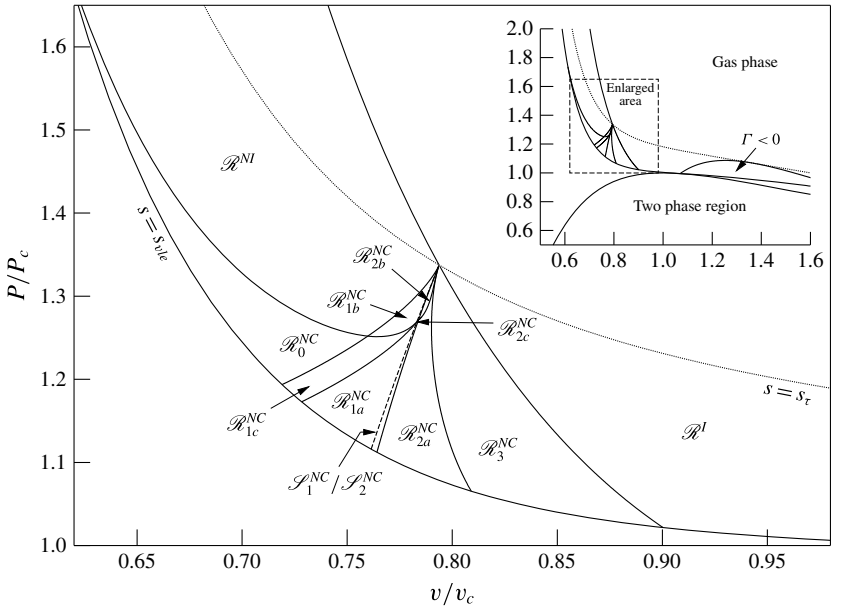

FIGURE 15. Thermodynamic map of the reservoir states leading to each functioning regime, computed from the van der Waals polytropic model with $c_v/R = 50$. Curves labelled $s = s_{vle}$ and $s = s_\tau$ represent the isentropes tangent to the vapour dome and to the $\Gamma = 0$ locus, respectively.

the entropy rise (including the potential transition $\mathscr{S}^{NI} \to \mathscr{S}^{I}$) would not qualitatively modify the flow. Thus, the qualitative differences between regimes $\mathscr{R}^{NI}$ and $\mathscr{R}^{I}$ are limited to the behaviour of the Mach number, which is inherited by the reservoir isentropic pattern. The latter condition is associated with other transitional loci of functioning regimes, see below.

If $s_{vle} < s_r < s_\tau$, all functioning regimes can possibly occur depending on the reservoir conditions. Similarly to case $\mathscr{R}^{NI}/\mathscr{R}^{I}$, a set of transitional curves for functioning regimes is coincident with its isentropic pattern counterpart. These transitions include $\mathscr{R}^{NC}_3/\mathscr{R}^{I}$, $\mathscr{R}^{NC}_2/\mathscr{R}^{NC}_3$, $\mathscr{R}^{NI}/\mathscr{R}^{NC}_{1b}$ and $\mathscr{R}^{NC}_0/\mathscr{R}^{NC}_{1c}$. Transition $\mathscr{R}^{NC}_3/\mathscr{R}^{I}$ corresponds to $\mathscr{S}^{NC}_3/\mathscr{S}^{I}$ because functioning regimes $\mathscr{R}^{NC}_3$ and $\mathscr{R}^{I}$ differ simply in the isentropic evolution of the Mach number, which is dictated by the isentropic pattern of the related reservoir conditions. As discussed in §§ 3.4–3.5, functioning regimes of classes $\mathscr{R}^{NC}_1$ and $\mathscr{R}^{NC}_2$ require that the reservoir isentropic pattern includes three sonic points. Therefore, the transition between these flows and those including a single sonic point in the reservoir isentropic pattern is effected when the reservoir conditions exhibit either transitional pattern $\mathscr{S}^{NC}_2/\mathscr{S}^{NC}_3$ or $\mathscr{S}^{NI}/\mathscr{S}^{NC}_1$. In the first case transition $\mathscr{R}^{NC}_2/\mathscr{R}^{NC}_3$ occurs; the second case corresponds to transitions $\mathscr{R}^{NI}/\mathscr{R}^{NC}_{1b}$ and $\mathscr{R}^{NC}_0/\mathscr{R}^{NC}_{1c}$.

The remaining transitions are related to some specific non-isentropic features of the flow. First consider the transition between $\mathscr{R}^{NC}_1$ and $\mathscr{R}^{NC}_2$ functioning regimes. It was shown that flows expanding from reservoir conditions corresponding to three sonic point must include rarefaction shocks in order to attain arbitrarily large exit Mach numbers. In the case of $\mathscr{R}^{NC}_2$ flows, the rarefaction shock is sonic on the upstream side and it is located in the converging section of the nozzle. In flows of type $\mathscr{R}^{NC}_1$, the rarefaction shock is sonic on the downstream side and it lies in the diverging

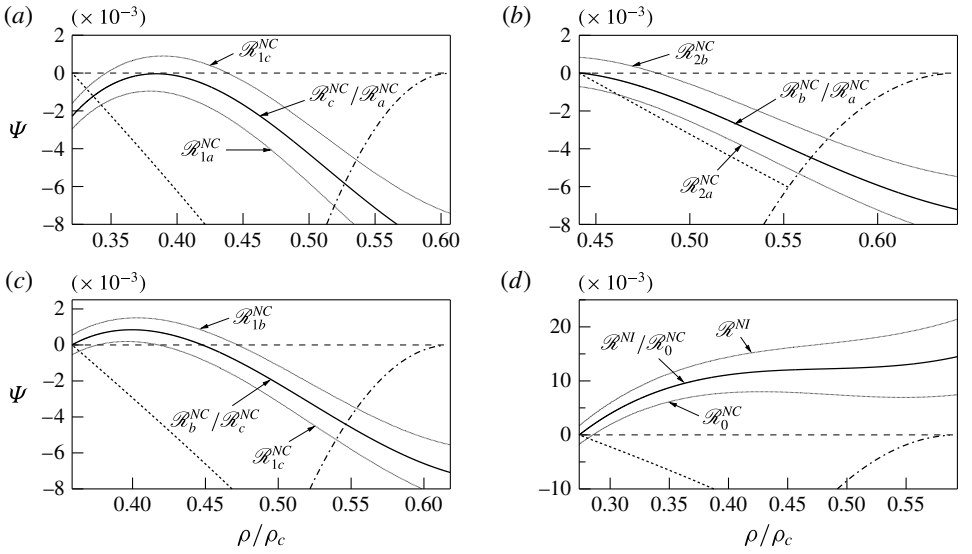

FIGURE 16. Exemplary transitional curves in the Ψ–ρ diagram: (*a*) $\mathscr{R}^{NC}_{c}/\mathscr{R}^{NC}_{a}$; (*b*) $\mathscr{R}^{NC}_{b}/\mathscr{R}^{NC}_{a}$; (*c*) $\mathscr{R}^{NC}_{b}/\mathscr{R}^{NC}_{c}$; (*d*) $\mathscr{R}^{NI}/\mathscr{R}^{NC}_{0}$. Also shown are the sonic locus (-·-·-·-) and the sonic shock disintegration (SD) locus (·····).

section of the nozzle. The transitional regime between these two classes exhibits a double-sonic shock, i.e. a shock which has both pre-shock and post-shock sonic states (see Thompson & Lambrakis 1973; Kluwick 2001; Zamfirescu, Guardone & Colonna 2008), exactly located at the throat section. In this respect, the transitional locus $\mathscr{R}^{NC}_{1}/\mathscr{R}^{NC}_{2}$ gathers all such reservoir states from which a double-sonic shock may possibly occur. As we can see from figure 15, the curves $\mathscr{R}^{NC}_{1}/\mathscr{R}^{NC}_{2}$ and $\mathscr{S}^{NC}_{1}/\mathscr{S}^{NC}_{2}$ are not coincident. As a consequence, reservoir states corresponding to $\mathscr{S}^{NC}_{2}$ pattern may in fact result in one of the $\mathscr{R}^{NC}_{1}$ functioning regimes. Admittedly, the latter condition occurs in a very limited range of pressure and density values; nonetheless it is further evidence of the fact that isentropic analysis alone is not sufficient for the correct prediction of such non-classical flows. Two additional transitional loci are sketched in figure 15. One is the curve associated with transition $\mathscr{R}^{NC}_{c}/\mathscr{R}^{NC}_{a}$, which requires that a shock wave featuring $\Psi = 0$ and $\mathrm{d}\Psi/\mathrm{d}\rho = 0$ is formed, see figure 16(*a*). That is, this shock has downstream sonic state and it is also a stationary point for Ψ. The last transitional curve involves $\mathscr{R}^{NC}_{2b}/\mathscr{R}^{NC}_{2a}$, $\mathscr{R}^{NC}_{2b}/\mathscr{R}^{NC}_{2c}$, $\mathscr{R}^{NC}_{1b}/\mathscr{R}^{NC}_{1c}$ and $\mathscr{R}^{NI}/\mathscr{R}^{NC}_{0}$. These transitions all have in common the occurrence of a post-sonic compression shock featuring $\Gamma = 0$ at the post-shock state, which is verified if $\Psi = 0$ at the lower endpoint of the density interval where Ψ is defined, see figure 16(*b–d*) for exemplary cases.

Inspection of figure 15 reveals that reservoir thermodynamic states resulting in non-classical flow regimes lie in a range of pressures and temperatures corresponding to supercritical fluid conditions. In particular, the temperature in the reservoir associated with stagnation states leading to non-classical regimes varies from $1.01 \lesssim T/T_c \lesssim 1.04$ according to the van der Waals model. Note, however, that the extension of the negative-Γ region and, in turn, of the thermodynamic region of reservoir states related to non-classical regimes is overestimated by the van der Waals thermodynamic model employed in the present work, if compared to more sophisticated equations of state (see e.g. Thompson & Lambrakis 1973).

The computed reservoir conditions leading to non-classical regimes are expected to lie in a range of temperatures above the thermal stability limit of the working fluid (see Calderazzi & Colonna 1997; Colonna & Silva 2003; Colonna *et al.* 2007; Pasetti, Invernizzi & Iora 2014). Therefore, in a future attempt to observe non-classical nozzle flows, an experimental set-up consisting of a nozzle directly connected to a reservoir appears to be impracticable. On the other hand, in order to avoid thermal decomposition, a viable experiment could be devised in which the stagnation enthalpy of the fluid is increased via heating and/or compression by external means before entering the nozzle, using for example a compressor, while keeping the static temperature below the thermal decomposition limit. In this respect, among candidate BZT fluids, siloxanes are possibly the best class of fluids for experiments and applications involving non-classical gasdynamic phenomena (see Colonna *et al.* 2007). Experimental investigations (see Angelino & Invernizzi 1993; Colonna 1996) indicate that siloxanes in stainless steel vessels are thermally stable at the temperatures characterizing states that are expected to support negative nonlinearities, provided that the fluid is sufficiently purified (see also Pasetti *et al.* 2014).

5. Conclusions

Steady flows of mono-component single-phase BZT fluids in a converging–diverging nozzle were investigated within the quasi-one-dimensional approximation. These flows were computed by solving an implicit equation for the density distribution along smooth isentropic branches of the solutions and by connecting these with the Rankine–Hugoniot jump relations. Fluids of moderate molecular complexity are found to exhibit non-monotone evolution of the Mach number in isentropic flows. If the molecular complexity is large enough to generate a thermodynamic region where Γ is negative, as many as three sonic points possibly occur. Isentropic analysis resulted in the definition of five different isentropic patterns corresponding to quasi-one-dimensional flows in a converging–diverging nozzle. In addition, non-classical effects include the admissibility of rarefaction shocks, of shock waves that are sonic either on the upstream or downstream side and of compression shocks splitting into two distinct entities (split-shock configuration).

Nozzle flows were classified according the layout of the exact solutions associated with flows expanding from a reservoir with fixed thermodynamic state into a stationary atmosphere. Starting from reservoir conditions corresponding to the five different isentropic patterns, as many as 10 different functioning regimes were identified. The complexity of the map of functioning regimes is due to the occurrence of shock-induced transitions of the isentropic pattern. It was shown that these transitions, in order to occur in the direction of increasing entropy, must follow a specific sequence. Notably, admissible transitions of the isentropic pattern may either increase or decrease the number of sonic points, leading to significant modification of the flow behaviour.

A thermodynamic map of the reservoir conditions resulting in each functioning regime was produced, in order to identify the thermodynamic region of interest for the observation of non-classical nozzle flows. A one-to-one correspondence between the isentropic pattern of the reservoir conditions and the functioning regime exists only between $\mathscr{S}^{I}$ and $\mathscr{R}^{I}$ and between $\mathscr{S}_3^{NC}$ and $\mathscr{R}_3^{NC}$. Note, for instance, that conditions were reported under which reservoir states of type $\mathscr{S}_2^{NC}$ lead to regime $\mathscr{R}_{1a}^{NC}$. This contrasts with the results obtained by previous authors based on the phase plane analysis only. Moreover, reservoir states in the $\mathscr{S}^{NI}$ region are found to include

non-classical flow features such as the split-shock configuration, e.g. $\mathscr{R}_0^{NC}$ functioning regime, although the phase plane corresponding to reservoir conditions is of the classical type (one sonic point).

Reservoir states resulting in non-classical nozzle flows are predicted to be at slightly supercritical conditions, namely, $1.01 \lesssim T/T_c \lesssim 1.04$. In these conditions, candidate BZT fluids are expected to decompose due to thermal breakdown and therefore the possibility of observing non-classical nozzle flows originating from still reservoir states is questionable. However, the stagnation enthalpy can possibly be increased locally by introducing e.g. a compressor along the expansion path.

The conclusions drawn in this work under the polytropic van der Waals model are expected to be consistent with those of more complex models such as the Peng–Robinson, the Martin–Hou or the Span–Wagner. Nevertheless, a comprehensive study is needed to assess the latter claim and is left for future investigations. Also, the effect of the molecular complexity of the fluid remains to be examined. Moreover, due to the use of analytical models, the present results are valid only sufficiently away from the critical point region.

Acknowledgements

This research is supported by ERC Consolidator grant no. 617603, Project NSHOCK, funded under the FP7-IDEAS-ERC scheme. The first author acknowledges the contribution of N. William in drafting a preliminary map of the functioning regimes.

REFERENCES

ANGELINO, G. & INVERNIZZI, C. 1993 Cyclic methylsiloxanes as working fluids for space power cycles. *J. Solar Energy Engng* **115** (3), 130–137.

ARGROW, B. M. 1996 Computational analysis of dense gas shock tube flow. *Shock Waves* **6** (4), 241–248.

BATES, J. W. & MONTGOMERY, D. C. 1999 Some numerical studies of exotic shock wave behavior. *Phys. Fluids* **11** (2), 462–475.

BETHE, H. A. 1942 The theory of shock waves for an arbitrary equation of state. *Tech. Paper* 545. Office of Scientific Research and Development.

BORISOV, A. A., BORISOV, A. A., KUTATELADZE, S. S. & NAKORYAKOV, V. E. 1983 Rarefaction shock wave near the critical liquid–vapor point. *J. Fluid Mech.* **126**, 59–73.

BROWN, B. P. & ARGROW, B. M. 1997 Two-dimensional shock tube flow for dense gases. *J. Fluid Mech.* **349**, 95–115.

BROWN, B. P. & ARGROW, B. M. 2000 Application of Bethe–Zel'dovich–Thompson fluids in Organic Rankine Cycle engines. *J. Propul. Power* **16** (6), 1118–1123.

CALDERAZZI, L. & COLONNA, P. 1997 Thermal stability of r-134a, r-141b, r-13i1, r-7146, r-125 associated with stainless steel as a containing material. *Intl J. Refrig.* **20** (6), 381–389.

CHANDRASEKAR, D. & PRASAD, P. 1991 Transonic flow of a fluid with positive and negative nonlinearity through a nozzle. *Phys. Fluids* A **3** (3), 427–438.

COLONNA, P. 1996 Fluidi di lavoro multi componenti per cicli termodinamici di potenza (Multicomponent working fluids for power cycles). PhD thesis, Politecnico di Milano, Milano, Italy.

COLONNA, P., CASATI, E., TRAPP, C., MATHIJSSEN, T., LARJOLA, J., TURUNEN-SAARESTI, T. & UUSITALO, A. 2015 Organic Rankine cycle power systems: From the concept to current technology, applications, and an outlook to the future. *Trans. ASME J. Engng Gas Turbines Power* **137** (10), 100801.

COLONNA, P., GUARDONE, A. & NANNAN, N. R. 2007 Siloxanes: a new class of candidate Bethe–Zel'dovich–Thompson fluids. *Phys. Fluids* **19** (10), 086102.

COLONNA, P., GUARDONE, A., NANNAN, N. R. & ZAMFIRESCU, C. 2008 Design of the dense gas flexible asymmetric shock tube. *Trans. ASME J. Fluids Engng* **130** (3), 034501.

COLONNA, P. & SILVA, P. 2003 Dense gas thermodynamic properties of single and multi-component fluids for fluid dynamics simulations. *Trans. ASME J. Fluids Engng* **125** (3), 414–427.

CRAMER, M. S. 1991 Nonclassical dynamics of classical gases. In *Nonlinear Waves in Real Fluids* (ed. A. Kluwick), pp. 91–145. Springer.

CRAMER, M. S. & BEST, L. M. 1991 Steady, isentropic flows of dense gases. *Phys. Fluids* A **3** (4), 219–226.

CRAMER, M. S. & FRY, N. R. 1993 Nozzle flows of dense gases. *Phys. Fluids* A **5** (5), 1246–1259.

CRAMER, M. S. & KLUWICK, A. 1984 On the propagation of waves exhibiting both positive and negative nonlinearity. *J. Fluid Mech.* **142**, 9–37.

CRAMER, M. S. & SEN, R. 1986 Shock formation in fluids having embedded regions of negative nonlinearity. *Phys. Fluids* **29**, 2181–2191.

CRAMER, M. S. & SEN, R. 1987 Exact solutions for sonic shocks in van der Waals gases. *Phys. Fluids* **30**, 377–385.

EMANUEL, G. 1996 Analysis of a critical point with application to fluid mechanics. In *1st AIAA Theoretical Fluid Mechanics Meeting, New Orleans, LA*.

FERGASON, S. H., GUARDONE, A. & ARGROW, B. M. 2003 Construction and validation of a dense gas shock tube. *J. Thermophys. Heat Transfer* **17** (3), 326–333.

FERGASON, S. H., HO, T. L., ARGROW, B. M. & EMANUEL, G. 2001 Theory for producing a single-phase rarefaction shock wave in a shock tube. *J. Fluid Mech.* **445**, 37–54.

GUARDONE, A. 2007 Three-dimensional shock tube flows for dense gases. *J. Fluid Mech.* **583**, 423–442.

GUARDONE, A. & ARGROW, B. M. 2005 Nonclassical gasdynamic region of selected fluorocarbons. *Phys. Fluids* **17** (11), 116101.

GUARDONE, A., SPINELLI, A. & DOSSENA, V. 2013 Influence of molecular complexity on nozzle design for an organic vapor wind tunnel. *Trans. ASME J. Engng Gas Turbines Power* **135**, 042307.

GUARDONE, A., VIGEVANO, L. & ARGROW, B. M. 2004 Assessment of thermodynamic models for dense gas dynamics. *Phys. Fluids* **16** (11), 3878–3887.

HAYES, W. D. 1958 The basic theory of gasdynamic discontinuities. In *High Speed Aerodynamics and Jet Propulsion: Fundamentals of Gasdynamics* (ed. H. W. Emmons), vol. 3, pp. 416–481. Princeton University Press.

KLUWICK, A. 1993 Transonic nozzle flow of dense gases. *J. Fluid Mech.* **247**, 661–688.

KLUWICK, A. 2001 Rarefaction shocks. In *Handbook of Shock Waves*, chap. 3.4, pp. 339–411. Academic.

KLUWICK, A. 2004 Internal flows of dense gases. *Acta Mech.* **169**, 123–143.

KUTATELADZE, S. S., NAKORYAKOV, V. E. & BORISOV, A. A. 1987 Rarefaction waves in liquid and gas-liquid media. *Annu. Rev. Fluid Mech.* **19**, 577–600.

LAMBRAKIS, K. C. & THOMPSON, P. A. 1972 Existence of real fluids with a negative fundamental derivative Γ. *Phys. Fluids* **15** (5), 933–935.

LAX, P. D. 1957 Hyperbolic systems of conservation laws II. *Commun. Pure Appl. Maths* **10** (4), 537–566.

LEVELT-SENGERS, J. M. H. 1970 Scaling predictions for thermodynamic anomalies near the gas-liquid critical point. *Ind. Engng Chem. Fundam.* **9** (3), 470–480.

LEVELT-SENGERS, J. M. H., GREER, W. L. & SENGERS, J. V. 1976 Scaled equation of state parameters for gases in the critical region. *J. Phys. Chem. Ref. Data* **5** (1), 1–51.

LEVELT-SENGERS, J. M. H., MORRISON, G. & CHANG, R. F. 1983 Critical behavior in fluids and fluid mixtures. *Fluid Phase Equilib.* **14**, 19–44.

MARTIN, J. J. & HOU, Y. C. 1955 Development of an equation of state for gases. *AIChE J.* **1** (2), 142–151.

MARTIN, J. J., KAPOOR, R. M. & DE NEVERS, N. 1959 An improved equation of state for gases. *AIChE J.* **5** (2), 159–160.

MATHIJSSEN, T., GALLO, M., CASATI, E., NANNAN, N. R., ZAMFIRESCU, C., GUARDONE, A. & COLONNA, P. 2015 The flexible asymmetric shock tube (FAST): a Ludwieg tube facility for wave propagation measurements in high-temperature vapours of organic fluids. *Exp. Fluids* **56** (10), 1–12.

MENIKOFF, R. & PLOHR, B. J. 1989 The Riemann problem for fluid flow of real materials. *Rev. Mod. Phys.* **61** (1), 75–130.

MÜLLER, S. & VOß, A. 2006 The Riemann problem for the Euler equations with nonconvex and nonsmooth equation of state: construction of wave curves. *SIAM J. Sci. Comput.* **28** (2), 651–681.

NANNAN, N. R., GUARDONE, A. & COLONNA, P. 2013 On the fundamental derivative of gas dynamics in the vapor–liquid critical region of single-component typical fluids. *Fluid Phase Equilib.* **337**, 259–273.

NANNAN, N. R., GUARDONE, A. & COLONNA, P. 2014 Critical point anomalies include expansion shock waves. *Phys. Fluids* **26** (2), 021701.

NANNAN, N. R., SIRIANNI, C., MATHIJSSEN, T., GUARDONE, A. & COLONNA, P. 2016 The admissibility domain of rarefaction shock waves in the near-critical vapour–liquid equilibrium region of pure typical fluids. *J. Fluid Mech.* **795**, 241–261.

OLEINIK, O. 1959 Uniqueness and stability of the generalized solution of the Cauchy problem for a quasi-linear equation. *Usp. Mat. Nauk* **14** (2), 165–170.

PASETTI, M., INVERNIZZI, C. & IORA, P. 2014 Thermal stability of working fluids for Organic Rankine Cycles: an improved survey method and experimental results for cyclopentane, isopentane and n-butane. *Appl. Therm. Engng* **73** (1), 764–774.

PENG, D. Y. & ROBINSON, D. B. 1976 A new two-constant equation of state. *Ind. Engng Chem. Fundam.* **15**, 59–64.

SPAN, R. & WAGNER, W. 2003*a* Equations of state for technical applications. I. Simultaneously optimized functional forms for nonpolar and polar fluids. *Intl J. Thermophys.* **24** (1), 1–39.

SPAN, R. & WAGNER, W. 2003*b* Equations of state for technical applications. II. Results for nonpolar fluids. *Intl J. Thermophys.* **24** (1), 41–109.

SPINELLI, A., DOSSENA, V., GAETANI, P., OSNAGHI, C. & COLOMBO, D. 2010 Design of a test rig for organic vapours. In *ASME Turbo Expo 2010: Power for Land, Sea and Air GT2010*.

SPINELLI, A., PINI, M., DOSSENA, V., GAETANI, P. & CASELLA, F. 2013 Design, simulation, and construction of a test rig for organic vapours. *Trans. ASME J. Engng Gas Turbines Power* **135**, 042303.

THOMPSON, P. A. 1971 A fundamental derivative in gasdynamics. *Phys. Fluids* **14** (9), 1843–1849.

THOMPSON, P. A. 1988 *Compressible Fluid Dynamics*. McGraw-Hill.

THOMPSON, P. A. 1991 Liquid–vapor adiabatic phase changes and related phenomena. In *Nonlinear Waves in Real Fluids* (ed. A. Kluwick), pp. 147–213. Springer.

THOMPSON, P. A., CAROFANO, G. C. & KIM, Y. G. 1986 Shock waves and phase changes in a large-heat-capacity fluid emerging from a tube. *J. Fluid Mech.* **166**, 57–92.

THOMPSON, P. A. & LAMBRAKIS, K. C. 1973 Negative shock waves. *J. Fluid Mech.* **60**, 187–208.

VAN DER WAALS, J. D. 1873 Over de continuïteit van den gas – en vloeistoftoestand (On the continuity of the gas and liquid state). PhD thesis, Leiden University, The Netherlands.

WENDROFF, B. 1972 The Riemann problem for materials with nonconvex equations of state I: isentropic flow. *J. Math. Anal. Appl.* **38** (2), 454–466.

WEYL, H. 1949 Shock waves in arbitrary fluids. *Commun. Pure Appl. Maths* **2** (2–3), 103–122.

ZAMFIRESCU, C. & DINCER, I. 2009 Performance investigation of high-temperature heat pumps with various BZT working fluids. *Thermochim. Acta* **488** (1), 66–77.

ZAMFIRESCU, C., GUARDONE, A. & COLONNA, P. 2008 Admissibility region for rarefaction shock waves in dense gases. *J. Fluid Mech.* **599**, 363–381.

ZEL'DOVICH, Y. B. 1946 On the possibility of rarefaction shock waves. *Zh. Eksp. Teor. Fiz.* **4**, 363–364.